5-2019

A Photometric Study of the Eclipsing Binary V574 Lyrae

Abigail L.J. Rickards
Stephen F Austin State University, theabigailrickards@gmail.com

A Photometric Study of the Eclipsing Binary V574 Lyrae

Creative Commons License

A PHOTOMETRIC STUDY OF THE ECLIPSING BINARY V574 LYRAE

by

ABIGAIL L. J. RICKARDS, Bachelor of Science

presented to the Faculty of the Graduate School of

Stephen F. Austin State University

In Partial Fulfillment

Of the Requirements

For the Degree of

Master of Science

STEPHEN F. AUSTIN STATE UNIVERSITY

May, 2019

A PHOTOMETRIC STUDY OF THE ECLIPSING BINARY V574 LYRAE

by

ABIGAIL L. J. RICKARDS, Bachelor of Science

APPROVED:

_____

Dr. Dan Bruton, Thesis Director

_____

Dr. Joseph Musser, Committee Member

_____

Dr. Norman Markworth, Committee Member

_____

Dr. Matthew Beauregard, Committee Member

_____

Dr. Pauline M. Sampson
Dean of Research and Graduate Studies

ABSTRACT

Variable stars provide unparalleled insight into stellar evolution and eclipsing binary variables are particularly excellent laboratories for determining stellar physical parameters and behavior. These parameters, when taken with those of other stars, can be used to evaluate current theories on stellar evolution and stellar structure. With the view of contributing useful data to this cause, a photometric study of the eclipsing binary system V574 Lyrae (Lyr) was undertaken to determine the system's physical parameters and to create a model of the system. Data were collected with a 0.36 m Ritchey-Chrétien telescope and the Sloan g', r', and i' filters and processed using Maxim DL and Mira Pro x64 image processing software. The resulting light curves were used with the Wilson-Devinney program to successfully determine the physical parameters of the system and model the stars.

ACKNOWLEDGEMENTS

Mr. Michaels: for sharing your observatory, knowledge, time, and home with me. Thank you for entertaining a novice astronomer and teaching her all she knows about eclipsing binary stars and enabling her to pursue her curiosity without feeling behind for not knowing it already. Thank you even more so for being my thesis advisor in everything but name and for dedicating the time to do so without official recognition.

Dr. Bruton: many, many thanks for taking time out of your very busy schedule to be my thesis advisor. Thank you for being kind and encouraging as well as methodical in setting goals for this research project and for being willing to share your role, albeit unofficially, with Mr. Michaels.

To the entire SFA physics faculty: for putting up with the crazy girl who wanted to complete her masters in a year and a half, for rearranging class schedules and teaching special courses so that she could do so, and for not flipping out and telling her she couldn't when she had a baby.

Alex: for cooking me dinner, taking over my chores, giving up your leftovers for my lunches, staying up with me when I didn't want to do my homework, putting up with my absences and late evenings, supplying me with endless quantities of tea, ice cream, and hugs, encouraging me to start grad school and to keep going when we found out we were pregnant two months in. Once again, I am in awe as I discover more of the man who is my husband and I cannot believe that you are mine.

Bear: to my son, for putting up with at least slightly unhealthy quantities of caffeine and sugar for the duration of your time in utero, ruining my taste for coffee, increasing my love of dairy, and doing your unconscious best to arrive after my finals. You cut it close. After finals, for being my travel companion on the hour drives to SFA, for being my classroom, homework, and thesis writing buddy, and for being the second most-loved man in my life. You deserve an honorary masters!

God: for creating and sustaining the universe I am privileged to live in and for giving me a mind inquisitive enough to want to explore it, intelligent enough to learn some things about it, and ignorant enough not to be bothered that I can never understand it all.

TABLE OF CONTENTS

LIST OF TABLES

CHAPTER 1

Introduction

Looking up on a clear summer night, the sky seems crowded with millions of points of light. We call them stars. Where did they come from? What are they doing as they shine into the void? How long will they last? We may be simultaneously struck with the enormity of the universe and an insatiable desire to know more of it. Naïvely, we may assume that each point of light is a single star, but what we cannot see with our eyes, or often even a telescope, is that over 50% of the stars within our galaxy are in systems of pairs or more orbiting their combined center of mass. This is fortunate since these binary stars provide a window into the realm of stellar evolution. In particular, if the stars are orbiting such that they eclipse the light from the other, one can use binary stars as "labs" in which to determine their stellar properties and perhaps to glimpse their gravitational and electromagnetic interactions.

A study of star brightness, also known as photometry, of these eclipsing binary systems can result in the determination of orbital inclination, orbital eccentricity, relative sizes, shapes, surface brightnesses, and in the case of total eclipses, an accurate mass ratio of the stars involved. If the observation and resulting plot of brightness versus time, called a light curve, has high enough precision, other parameters can be determined, and when combined with a spectroscopic study of the system the photometric results can be reevaluated to find the specific masses of each star (Kallrath and Milone 1999). These parameters can be used in conjunction with those of other stars

to evaluate the current theories on stellar evolution and stellar structure and adjust the theories as necessary to reflect the physical reality observed in our universe.

Classification of Eclipsing Binary Stars

While all binary star systems involve two stars orbiting each, eclipsing binary systems alternately block light from the each other as viewed from Earth and consequently the brightness or magnitude of the system appears to change with time. The eclipse (whether an occultation or transit) of the hotter star by the cooler star results in the greater decrease in total magnitude and is termed the primary eclipse. The eclipse of the cooler star by the hotter star causes a shallower secondary eclipse. Observational light curves can be used to determine the time of minimum light without resolving the individual stars.

Early eclipsing binary classification schemes attempted to sort eclipsing binary systems purely on the appearance of their light curves. The three recognized categories were Algol, Beta Lyrae, and W Ursae Majoris (W UMa) type systems. Algol-type systems exhibited light curves with almost constant magnitude other than a deep minima at the primary eclipse and a much shallower minima at the secondary eclipse. Beta Lyrae and W Uma-type systems both exhibited continuous changes in magnitude. However, Beta Lyrae-types had minima of noticeably different depths while W UMa-types had minima of very similar depths. In any case, this classification system was troublesome as not a few binary systems exhibited characteristics overlapping one or more categories or not fitting any category.

Enter the Roche Model introduced by Kopal (1955). Based on the work of 19th

century mathematician E.A. Roche on the circular restricted three-body problem, the Roche model classifies binary star systems based on each star's gravitational equipotential surface (see Figure 1.1). Within this model there exist five Lagrangian points L_1 through L_5 at which a infinitesimal mass will remain at rest relative to the two stars. The equipotential surface that intersects the L_1 point is referred to as the Roche limit or inner potential and the two volumes enclosed by the surface are known as the Roche lobes. Similarly, the equipotential surface that intersects the L_2 point is termed the outer potential. It is relative to the Roche limit that binary star systems are classified in Kopal's scheme (1978). If both stars in a binary system have not filled their Roche lobes, the system is classified as a detached system. If one star has filled its Roche lobe, the system is classified as semi-detached and matter can leave the filled lobe through the L_1 point and possibly impact the other star. If both stars have filled their Roche lobes past the inner potential surface but not the outer potential, the system is classified as a contact system. Contact systems are known to exactly correspond to W UMa-type systems. Most binary systems can be classified into one of Kopal's three categories as long as their physical configurations can in some way be determined. Since most indiviudual stars can not be directly observed, some attempt must be made to model the light curve to ascertain the system's physical parameters.

W UMa-type binary systems are sometimes further subdivided into W-type and A-type systems. In general W-type systems are cooler and possess less stable orbital periods than do A-type systems (Rucinski 1973; Rucinski 1974). As contact binaries, the stars in both types share a common convective envelope which would suggest that each component reradiates about 50% of the light received from the other star (Lucy 1968; Rucinski 1969). However, Rucinksi (1974) suggests that A-type W UMa systems

3
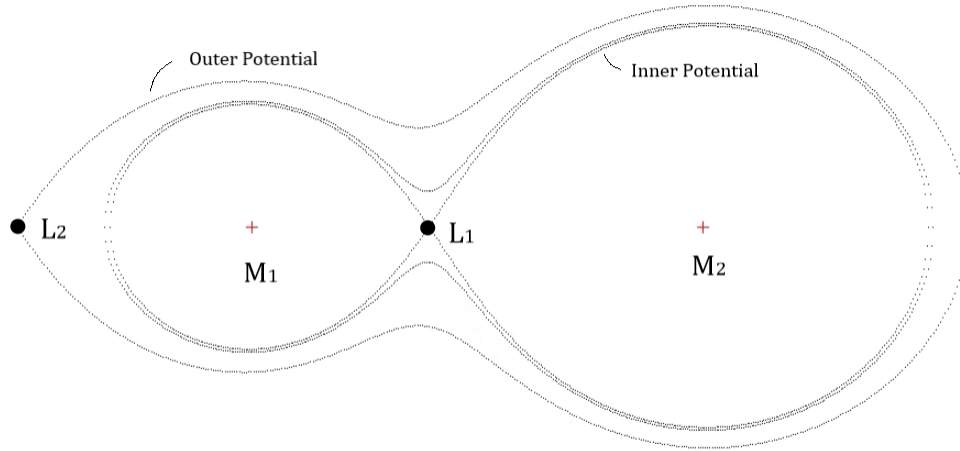
Figure 1.1: A representation of the inner and outer equipotentials for a binary with a mass ratio of 2.90 (M_2/M_1).

are unique in that the convective envelope is itself surrounded by a very thin radiative layer which would suggest each component reradiates 100% of the light received from the other star. The amount of light one star reradiates from the other is called bolometric albedo and is an important parameter in modeling a binary star system.

CCD Photometry

Methods of observation include visual, photoelectric, and CCD photometry. Photometry using a charge coupled device (CCD) imaging camera is currently the preferred method of photometric observation for astronomers. This is because CCDs not only have a linear correspondence between star magnitude and photon count but also have a wide enough field of view that comparison stars can be used to further increase

the precision of data. Each pixel within a CCD chip is a photoelectric well that has a region within which there is a linear response to the number of photons that strike the pixel. The exposure times of the observations can (and should) be tailored to make sure that the chip as a whole remains within its range of linear response. In addition, calibration frames called darks, biases, and flats should be taken with each observing run (Howell 2006). Dark frames are taken as a sixty second exposures (or longer) with the camera shutter closed and account for the effects of dark current and bad pixels within the chip. Bias frames are taken as zero second exposures with the shutter closed to measure the minimum noise in the CCD and camera circuity. Flat frames are taken with the telescope facing a uniformly illuminated surface. Flat fields are images of the optical noise in the system such as dust motes on the optical surfaces, reflections off of the inside of the telescope, vignetting, and pixel to pixel variations in sensitivity across the CCD. These calibration frames can be median combined and applied to each raw frame in order to remove the unwanted effects. When these calibration frames are used in conjunction with comparison stars and appropriate exposure times, high precision brightness measurements of a star can result.

CHAPTER 2

Target Selection

<u>Objectives</u>

The overarching objective of this project is to contribute the first multi-band photometric study of an eclipsing binary star. More detailed objectives in support of this goal are as follows:

1. Observe a yet unmodeled eclipsing binary star using CCD photometry.

2. Complete a period study of the eclipsing binary star. This involves determining times of minima from the light curves from each night and using these times together with all other published times of minima to create an observed minus calculated (O-C) time of minima diagram. This diagram is then used to determine the current period of the binary system by fitting a function to the residuals.

3. Determine the physical parameters of the eclipsing binary star from a computer solution to produce a synthetic light curve that closely matches the observed light curve and a 3D model of the binary star system.

<u>Selection Criteria</u>

In order to accomplish the above objectives a suitable target needed to be selected. AAVSO's International Variable Star Index (VSX) was used to collect information on possible target stars. Selection criteria included the following requirements:

1. The binary star system must have had an altitude of greater than thirty degrees at the onset of astronomical twilight on June 1, 2018, and at the conclusion of astronomical twilight on October 14, 2018, when observing from the latitude of Nacogdoches, Texas. This enabled research to take place over the summer of 2018 with some additional time available during the fall in case of inclement weather.

2. The listed period of the binary star system must have been approximately equal to or less than the shortest span of astronomical twilight occurring between June 1, 2018, and October 14, 2018, in order to observe an entire orbital cycle in one night of observation. This time span was found to be approximately 6.5 hr or 0.27 days. This criterion was aimed at minimizing the time required to complete the thesis research by reducing the number of nights of observation.

3. The minimum brightness of the star must have been less than apparent magnitude 14 in order to work within the limitations of the 0.36 m telescope at Waffelow Creek Observatory.

4. If available, systems with preexisting light curves that showed evidence of total eclipses were preferred as potential targets over those with partial eclipses. A total eclipse would allow for a more precise determination of the mass ratio.

7

5. The binary star system must not have been previously modeled in order for further modeling to generate original research. Additional consideration was given to systems that had no published multi-band light curves, light curve solutions, or period studies, but that did have published times of minima available to aid a period study.

Using the selection criteria listed and information from AAVSO's VSX nineteen potential targets were found and from these the final target star, V574 Lyr, was selected (Table 2.1).

Table 2.1: Coordinates of V574 Lyr.

Name	Right Ascension			Declination			Magnitude
	h	m	s	°	'	"	V
V574 Lyr	18	27	12.23	+36	14	36.7	12.05 - 12.66

<u>Literature Review</u>

An in-depth survey of the published works mentioning V574 Lyr utilized the Set of Identifications, Measurements, and Bibliography for Astronomical Data (SIMBAD), the NASA Astrophysics Data System (ADS), and Bob Nelson's Database of Eclipsing Binary O-C Files. V574 Lyr was originally discovered in 2000 by automatic algorithmic analysis of data from the Robotic Optical Transient Search Experiment I (ROTSE I) which automatically classified it as a contact binary system (Akerlof, *et al.* 2000). Since then V574 Lyr has been included in several catalogues of variable and eclipsing binary stars (Avvakumova, *et al.* 2013; Gettel, *et al.* 2006; Kazarovets, *et al.* 2003;

Malkov, *et al.* 2006; Pribulla, *et al.* 2003) as well as utilized in studies of automatic variable classification (Hoffman, *et al.* 2009), the outer galactic halo (Drake, *et al.* 2013), contamination of the Kepler Field (Coughlin, *et al.* 2014), and the evolutionary status of eclipsing binaries (Avvakumova and Malkov 2014). Additionally, at least thirty-one published articles have included times of minima of V574 Lyr. However, at this time there have been no published articles involving multi-wavelength photometry, modeling, or determination of parameters of this system.

CHAPTER 3

Instrumentation

Due to its demonstrated ability to attain milli-magnitude precision brightness measurements and to do so without the need for extensive configuration and alignment, the robotic telescope at the Waffelow Creek Observatory was chosen for data acquisition of the target star. This observatory is located on the nine miles northeast of Nacogdoches, Texas.

Hardware

The hardware in use at the Waffelow Creek Observatory is housed within a observatory building equipped with a sliding roof with a controller and motor by SkyRoof. To further protect the equipment, two weather stations, one by Davis Instruments and the other by SkyAlert, are located outside the building to detect inclement weather and allow time for the observatory to be shut down before it arrives.

Within the observatory is found a 0.36 m Ritchey-Chrétien telescope by Third Planet Optics (Figures 3.1 and 3.3). The telescope is equipped with a secondary mirror dew heater to combat inevitable condensation from the humid East Texas climate. The telescope is mounted on a Paramount MX robotic German equatorial mount by Software Bisque (Figure 3.1) equipped with magnetic switches that confirm that the telescope is homed before the roof is opened or closed. The mount itself is

set into an isolated concrete pier to reduce any vibrations from walking observers or air currents in and around the observatory. Attached to the telescope is a Model STXL-6303 CCD camera by SBIG which has a dedicated chip cooler to reduce thermal fluctuations within the chip (SBIG). Also attached to the telescope are Model FW83-STXL 50 mm filters by Astrodon and a Model TCF-S3 focuser by OPTEC. The filters used are the Sloan Digital Sky Survey photometric filters g', r' and i' which are widely recognized in astronomical research at this time (see Figure 3.2). Mounted to the interior wall of the observatory is a flat field light source by Spike-a which is used to take flat field calibration frames for the CCD camera (see Figure 3.3). The roof controller, weather stations, robotic mount, filters, focuser, and CCD camera are all connected via USB to a Windows PC remote desktop control station.
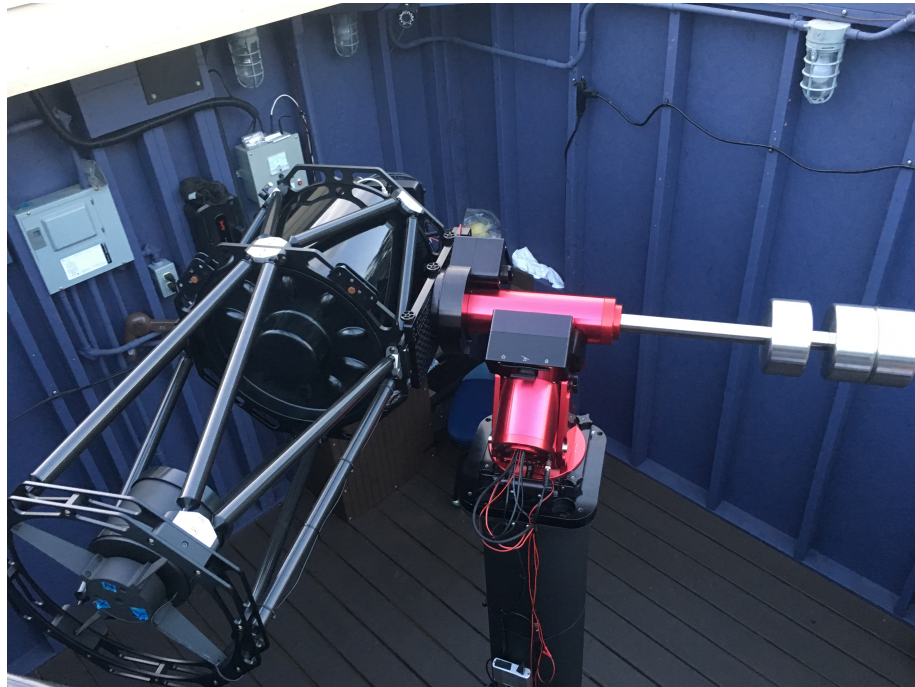
Figure 3.1: Bird's eye view of the telescope and German equatorial mount at Waffelow Creek Observatory.
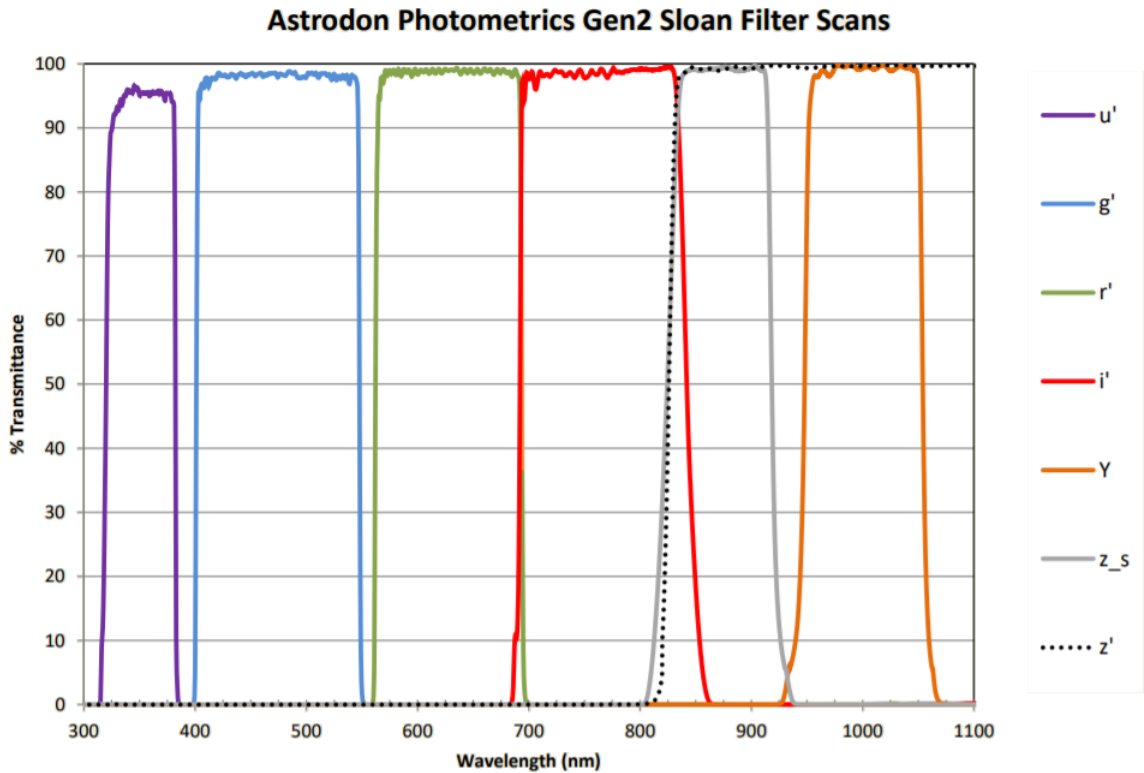
Figure 3.2: Astrodon's spectral responses of the Sloan Digital Sky Survey photometric filters (Astrodon).

Software

All systems at Waffelow Creek Observatory can be controlled from the remote desktop control station (see Figure 3.4). Each system is controlled by its respective software as follows: the roof controller and motor are controlled by SkyRoof software, the robotic telescope mount is controlled by TheSkyX software, the focuser is controlled by FocusMax 4.0 software, and the CCD camera, chip cooler, and filter selector are controlled by MaxImDL software.

While each system is controlled by a different program, all programs can be con-

Figure 3.3: Side view of the telescope and flat field at Waffelow Creek Observatory.

trolled by the Astronomer's Control Panel (ACP) program so that observing runs can be fully automated and the user does not have to be present after the initial set up and start of observations. A start up script "StartUpObs.js" run by ACP checks weather conditions, opens the roof, and establishes equipment connections with the various system control software. The script "AcquireImage.js" prompts the user to link to an observing plan file that specifies the exposure time of frames, start and end times of run, filter type, and target coordinates and the script then initiates the observing run. In the event of inclement weather signaled by the weather stations, ACP will home the telescope, shut the roof, save the current observations, and shut down all systems. Otherwise ACP will continue the observing plan as dictated in the plan file until the specified time to execute the shutdown sequence. The user

13

needs only to collect the saved images at the end of the run. However, it is wise to monitor the first few images for quality after starting the observation, and if one suspects a sudden or drastic temperature change overnight, it is also recommended to specify that ACP utilize the autofocus feature of FocusMax 4.0 one or more times during the run. Additionally, collected images should be inspected for cloud coverage or other unwanted interference such as cosmic ray hits and satellite and aircraft exposure streaks.
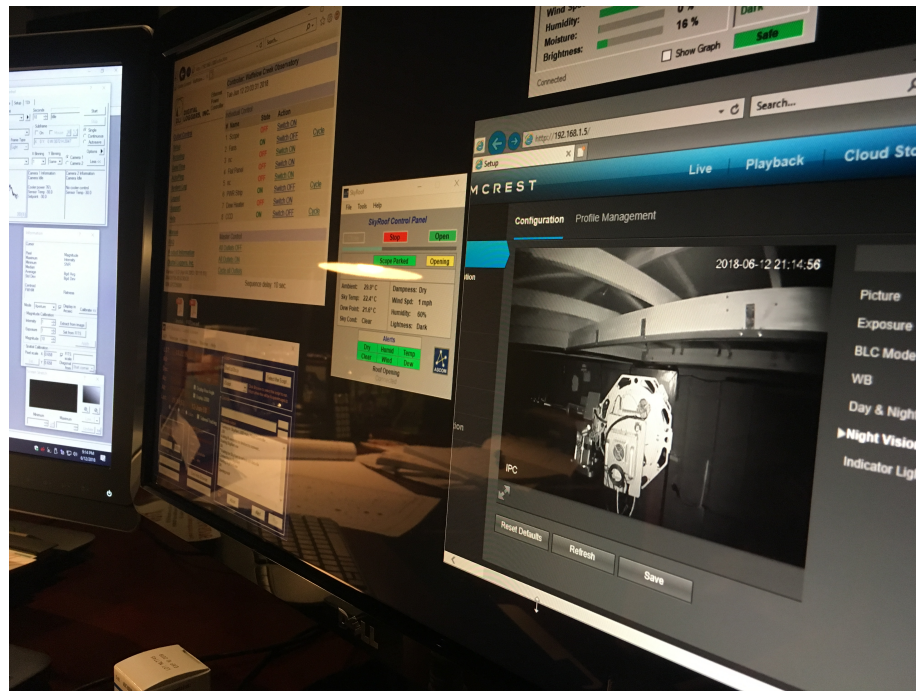
Figure 3.4: Desktop screen showing various programs controlling the Waffelow Creek Observatory.

CHAPTER 4

Observations

Data Collection

Observation runs utilized the software programs already in place for controlling the hardware of Waffelow Creek Observatory. The set-up protocol for a typical observing run took place from the desktop control center as follows:

1. Turned on the telescope fans, power strip, and CCD camera.

2. Using the camera control software Maxim DL, connected the CCD camera and turned on the cooler. The cooler needed to reach a steady -30.0 degrees Celsius to eliminate dark current in the chip before continuing set-up.

3. Using Maxim DL, thirty bias frames, fifteen dark frames, and fifteen flat frames were taken using an exposure time and filter corresponding to the filter to be used that night. These calibration frames were taken at the beginning of every run. The Sloan g', r', and i' filters were utilized for this photometric study.

4. Using the Astronomers Control Panel (ACP) software, script "StartUpObs.js" was run. This checked weather conditions, opened the roof, and established equipment connections with various controlling software.

5. Using the telescope control software TheSkyX, we first made sure the telescope had been connected, then homed the telescope. The homing process was mon-

itored via the surveillance camera. When home had been found, we input and slewed to the target star's coordinates.

6. Using the "Acquire Star" feature of FocusMax 4.0 software, we auto-focused the CCD camera. As the telescope and optics cooled to ambient temperature the focus shifted. The auto-focus process was repeated until observing run was about to begin.

7. Using Maxim DL, several test frames were taken using the chosen filter for the observing run and varying exposure time until the signal-to-noise ratio was 200:1 or higher. This was done to ensure that data would be able to reach milli-magnitude precision. Exposure time was noted for future reference and varied from night to night depending on the seeing and from filter to filter.

8. The template observing plan file was opened and the exposure time of frames, start and end times of run, filter type, and target coordinates to desired settings were adjusted. The file was then saved.

9. Using ACP, the "AcquireImage.js" script was run and the observing plan file was selected when prompted.

10. The first few frames of data were monitored and monitoring was continued as long as required to verify focus was stable. If weather forecasts indicated that temperature might significantly change during the night, plans were made to re-focus the camera mid-observing run. Otherwise the observation was allowed to continue unsupervised. ACP coordinated with the other software to automatically park the telescope and shut the observatory roof in the event of inclement

weather or the end time of the observing run being reached.

11. Image files were downloaded from the CCD camera to the computer as each image was acquired.

Data were collected over a total of thirteen nights with at least two nights of observation per filter in order to acquire data over a complete orbital period in each filter (see Table 4.1). Note that a second set of observations in both the g' and r' filters was completed in the event that the target star experienced a change in the location of any star spots in the interim between June and July observations. Resulting data were in the form of several hundred raw images per night saved as Flexible Image Transport System (FITS) files with almost 5000 total images collected (FITS). Data reduction using computer software was required to extract useful information from the raw image files.

Table 4.1: Dates of observation, filters used, and number of images collected.

Observation	Date	Filter	Images
1	6/12/18	r'	416
2	6/14/18	r'	406
3	6/15/18	g'	320
4	6/16/18	g'	356
5	7/13/18	i'	412
6	7/14/18	i'	412
7	7/15/18	r'	418
8	7/19/18	r'	397
9	7/20/18	g'	354
10	7/21/18	g'	308
11	7/31/18	g'	376
12	8/1/18	g'	334
13	8/2/18	g'	377

Data Reduction

Data reduction occurred in several stages. The first stage utilized AAVSO's star chart of the target star and data from the Panoramic Survey Telescope and Rapid Response System (Pan-STARRS) database to select comparison stars and a check star. These stars should have a constant known magnitude and be of similar magnitude and color to the target star. Mira Pro x64 image processing software (Mira) can use these stars to accurately calibrate and determine apparent magnitudes of the target star in all three filters through the process of ensemble differential photometry (AAVSO 2014). In addition, these stars needed to be uniformly distributed around the target star in order for the ensemble differential photometry to be able to also account for any CCD camera defects. Color comparison of the stars was completed by comparing the difference between the g' and r' magnitudes of the target, check, and comparison stars. Nonvariability of the comparison stars will be confirmed if check star photometry produces a light curve of constant magnitude in agreement with its accepted apparent magnitude. Twelve comparison stars and one check star were selected and are listed in Table 4.2.

Images were then examined for outlying data. Sky conditions recorded by the video camera SkyCam at the SFASU Observatory were used to judge whether or not to remove frames due to excessive cloud coverage. In addition, raw images were examined for cosmic ray strikes or aircraft exposure streaks near the comparison and target stars. Such frames were removed from the data set.

Next, the dark, bias, and flat frames from the beginning of an observing run were compiled via pixel-by-pixel averaging into a master dark, master bias, and master

Table 4.2: Comparison and check star coordinates and magnitudes.

Name	Type	RA	DEC	Sloan Filter		
		(h)	(°)	g'	r'	i'
GSC 2636:1762	Comparison	18.45432	36.20348	13.411	13.093	12.397
GSC 2635:0832	Comparison	18.44609	36.35452	13.663	12.729	12.991
GSC 2636:1917	Comparison	18.46325	36.16433	13.152	12.704	12.559
GSC 2636:1723	Comparison	18.45344	36.08804	13.586	12.854	12.555
GSC 2636:1732	Comparison	18.45773	36.08907	13.557	12.954	12.668
GSC 2636:1902	Comparison	18.46575	36.35767	13.884	13.137	12.696
GSC 2635:1050	Comparison	18.43789	36.24928	13.461	12.725	12.300
GSC 2636:1638	Comparison	18.45698	36.34613	12.312	11.503	11.196
GSC 2635:1104	Comparison	18.44038	36.13918	13.317	12.751	12.418
GSC 2635:1269	Comparison	18.44211	36.12028	12.454	11.722	11.439
GSC 2635:1292	Comparison	18.44552	36.09571	13.137	12.791	12.666
GSC 2636:1944	Comparison	18.45129	36.11665	11.951	11.357	11.097
GSC 2635:1284	Check	18.44672	36.30038	12.755	12.468	12.380

flat using Mira. The master dark and master bias were subtracted from each data exposure which was then divided by the master flat for that filter. This procedure was repeated for each of the thirteen total observing runs.

The list of comparison stars along with their coordinates and magnitudes was input into Mira. Mira took readings of sky brightness from the user-specified annulus around each star (comparison, check, and target) and subtracted these from the brightness of the corresponding star. The resulting brightnesses were then compared with the known apparent magnitudes of the comparison stars to extract the photometric data via ensemble differential photometry while simultaneously correcting for any remaining chip defects or atmospheric effects. Ensemble differential photometry involves first finding the measured magnitudes of the target, check, and comparison stars from the gain, image exposure time, and photon counts within each star's annulus. Differential magnitudes are the found by subtracting the measured magnitude

19

of a comparison star from the measured of magnitude of the target (or check) star. A standard magnitude of the target (or check) star is found by adding the differential magnitude from comparison star to the published standard magnitude of the check star. These standard magnitudes are then combined via a weighted average into an average standard magnitude for the target (or check) star. These data were saved in tab-delimited format and then were transferred to Microsoft Excel for further processing.

However, issues were encountered when using Mira to process the images and extract photometric data. The Heliocentric Julian Dates (HJD) of the photometric data were found to be changed to incorrect values. However, the date recorded in each FITS header of the raw and processed images was correct indicating that the date was being overwritten at some point after the processing of the images but before (or during) the extraction of the photometric data. In general, each frame date was being shifted approximately five minutes behind the actual date the frame was taken. An example of the discrepancy noticed is given in Table 4.3 where the "calculated JD" and "calculated HJD" were found from Dr. Dan Bruton's (2018) javascript HJD calculator. After many attempts to locate and correct the appropriate photometry setting(s) within Mira and after uninstalling and reinstalling Mira, it was eventually found that the issue was limited to one computer and that completing the photometric analysis on a different computer resolved the issue.

Table 4.3: Reported times of observation of exposure #13 from 06/12/18 throughout various steps of data processing.

Source	Reported Date
Image Date Observed	6/12/18 03:00:42 UT
Calculated JD	2458282.6254861
Calculated HJD	2458282.628307
Raw Image HJD	2458282.628307
Processed Image HJD	2458282.628307
Photometric HJD	2458282.624921

Observations of V574 Lyr

After the data were reprocessed and confirmed to have the correct HJD, the data were transferred to Microsoft Excel where they were sorted into a more usable format and used to generate light curves of the check and target stars. Orbital phase was calculated via the equation shown below, where T is the HJD of an observation, T_o is a user specified epoch or time of primary minimum, and P is the orbital period of the system.

$$\phi = \frac{T - T_o}{P} - Int\left(\frac{T - T_o}{P}\right)$$

Folded light curves for each filter were generated by plotting all data runs for that filter versus orbital phase. The result was Figure 4.1 in which the reader can observe the light curves from the g', r' and i' data as well as a qualitative plot of the check star r' magnitude with respect to the target's phase. Note that the magnitude of the check star does indeed remain constant and the comparison stars were nonvariable as is expected if quality photometry has been performed. Light curves from individual

observations can be found in Appendix A.
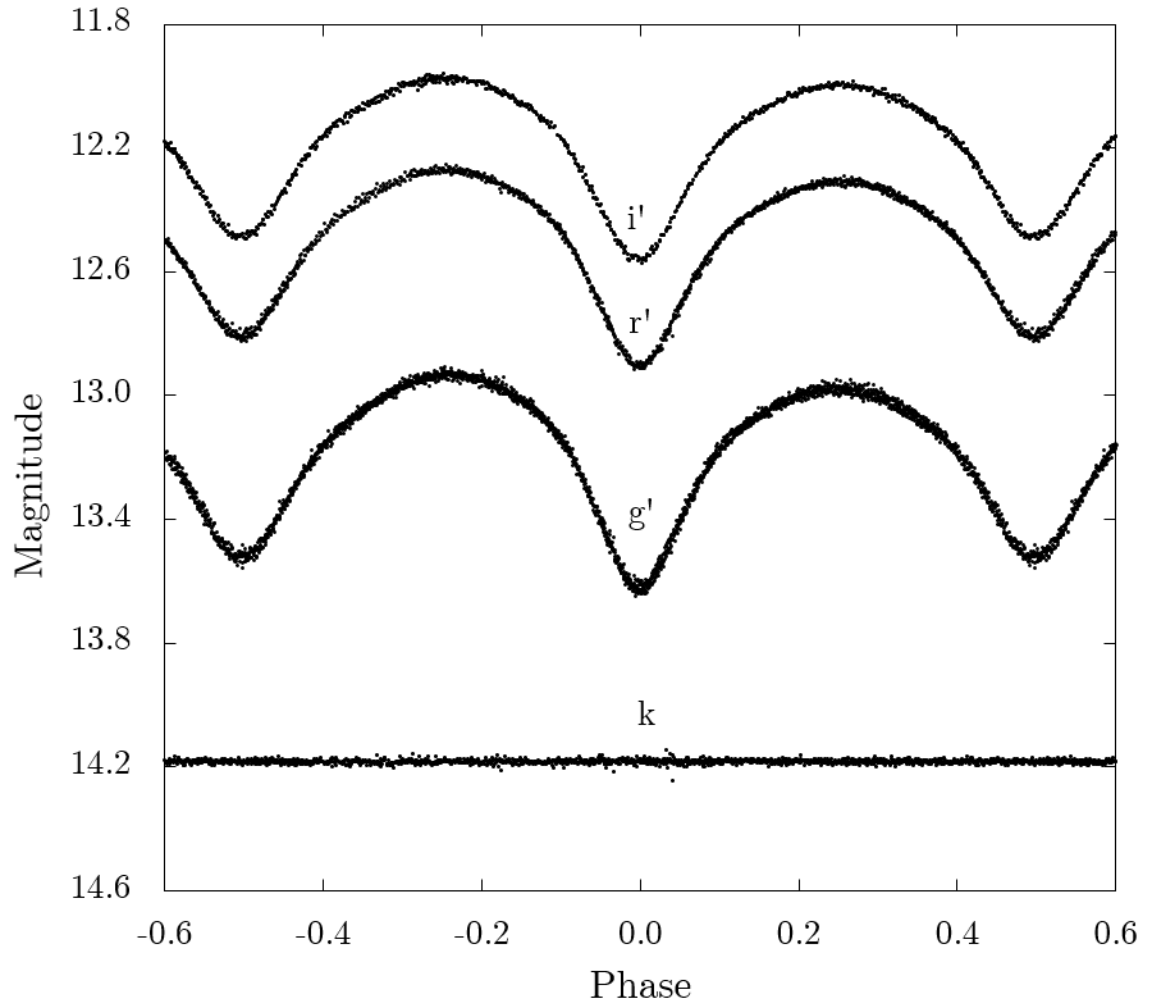
Figure 4.1: Folded light curves for the g', r', and i' passbands.

CHAPTER 5

Period Study

With collection of observational light curves comes the possibility of determining new times of primary and secondary eclipse or times of minima. These new times of minima combined with minima times from other observers can be incorporated into a period study. This type of study can be used to determine a current orbital period of the two stars, as well as to discern trends in period changes due to possible mass transfer, presence of a third body, non-spherical mass distribution, or general relativistic effects (Kallrath and Milone 1999).

Method

Each observational light curve was analyzed to find times of minima for the primary and secondary eclipses using the Minima v2.3 program (Minima v2.4). This program prompts the user to upload a section of the observational light curve data corresponding to a primary or secondary eclipse–for a primary eclipse the data between 0.85 phase to 0.15 phase was chosen and for a secondary eclipse between 0.35 phase to 0.65 phase. Once the data are input in comma separated variable (.csv) format, the program allows the user to find the time of minima via six different methods: parabolic fit, tracing paper method, bisection of chords method, Kwee and van Woerden fit, Fourier fit, and sliding integration method. After the time of minima

has been determined by all six methods, Minima v2.3 allows the user to select which methods to use in calculating an average time of minima. For this study, all six methods and their errors were used to compute an average time of minima for each eclipse.

From the thirteen nights of data, twenty new times of minima were determined and are listed in Table 5.1. These observed times of minima were compiled with a general survey of all published times of minima for the target star (see Appendix A, Table B.1) and recorded in a Microsoft Excel spreadsheet for a total of one hundred and thirty-seven times of minima observed from 1999 to 2018. Since there have been no previous period studies performed on V574 Lyr, the general linear ephemeris

$$JD(prim)_{hel} = 2457576.53298 + 0.273127E \qquad (5.1)$$

was used to calculate times of minima, T_{min}, of primary and secondary eclipses with T_0, the zero epoch, being chosen to be HJD 2457576.53298 ± 0.0001 from the observations of Jurysek, *et al.* (2017), P representing the current accepted period of 0.273127 days from Kreiner's TIming DAtabase at Krakow (TIDAK) (2004), and E representing the number of integer cycles for primary eclipses or half integer cycles for secondary eclipses before or after the zero epoch. The results of the observed minima minus the calculated minima (O-C) were plotted versus the number of elapsed cycles and linear and quadratic regression analyses were conducted on the data. If the fit is linear, this indicates that the actual period of the system is constant but the currently accepted value of the period is inaccurate. The correction of the period will be the slope of the regression line. A quadratic (or higher polynomial) approximation

indicates an orbital period increasing or decreasing linearly with time, possibly due to mass transfer between the stars or the loss of mass from the system (Sterken 2005).

Table 5.1: Observed times of minima of V574 Lyr (Rickards 2018).

Type	Time of Minima (HJD)	Error (dys)
II	2458282.70406	0.00005
I	2458284.75360	0.00004
I	2458285.84615	0.00005
II	2458285.70856	0.00004
I	2458286.66566	0.00005
II	2458286.80091	0.00004
I	2458313.70496	0.00005
II	2458313.84114	0.00005
I	2458314.79757	0.00004
II	2458314.66064	0.00004
I	2458315.89035	0.00004
II	2458315.75290	0.00005
I	2458319.71411	0.00006
II	2458319.84992	0.00005
I	2458320.80653	0.00005
II	2458320.66926	0.00005
I	2458331.73153	0.00005
I	2458332.82435	0.00005
II	2458332.68679	0.00005
I	2458333.64364	0.00004
II	2458333.77951	0.00006

Results

After completing both a linear and quadratic regression analysis on the O-C diagram, it was found that a quadratic regression better approximated the data. The linear regression shown in Figure 5.1 only yielded an R-value of 0.287 indicating a

poor approximation. The resulting linear ephemeris is

$$JD(pri)_{hel} = 2458333.6412 + 0.27312711E. \tag{5.2}$$
$$\pm \quad 3 \quad \pm \quad \quad 3 \tag{5.3}$$

The quadratic regression shown in Figure 5.2 provided an R-squared value of 0.668 and an adjusted R-squared value of 0.663 indicating sufficient correlation to indicate that the period of the system is changing. The resulting ephemeris was found to be

$$JD(pri)_{hel} = 2458333.6438 + 0.27312788E + 3.4 \times 10^{-11}E^2. \tag{5.4}$$
$$\pm \quad 2 \quad \pm \quad \quad 7 \quad \pm 3 \tag{5.5}$$

From this ephemeris an adjusted period of 0.27312788 days and epoch of HJD 2458333.6438 are found. In addition, it is found that the period is increasing by approximately 0.79 ± 0.06 seconds per century. Indeed, it should not be surprising that the orbital period is changing since this a common characteristic of W UMa type binaries.

Note that the residuals of the quadratic regression shown in Figure 5.2 give some indication that the orbital period of V574 Lyr has experienced sudden or perhaps periodic changes superimposed on the linear change of orbital period. While an approximation that accounts for these changes would be preferable, there are insufficient data to justify pursuing a better fit by means of piecewise linear or higher polynomial fits.
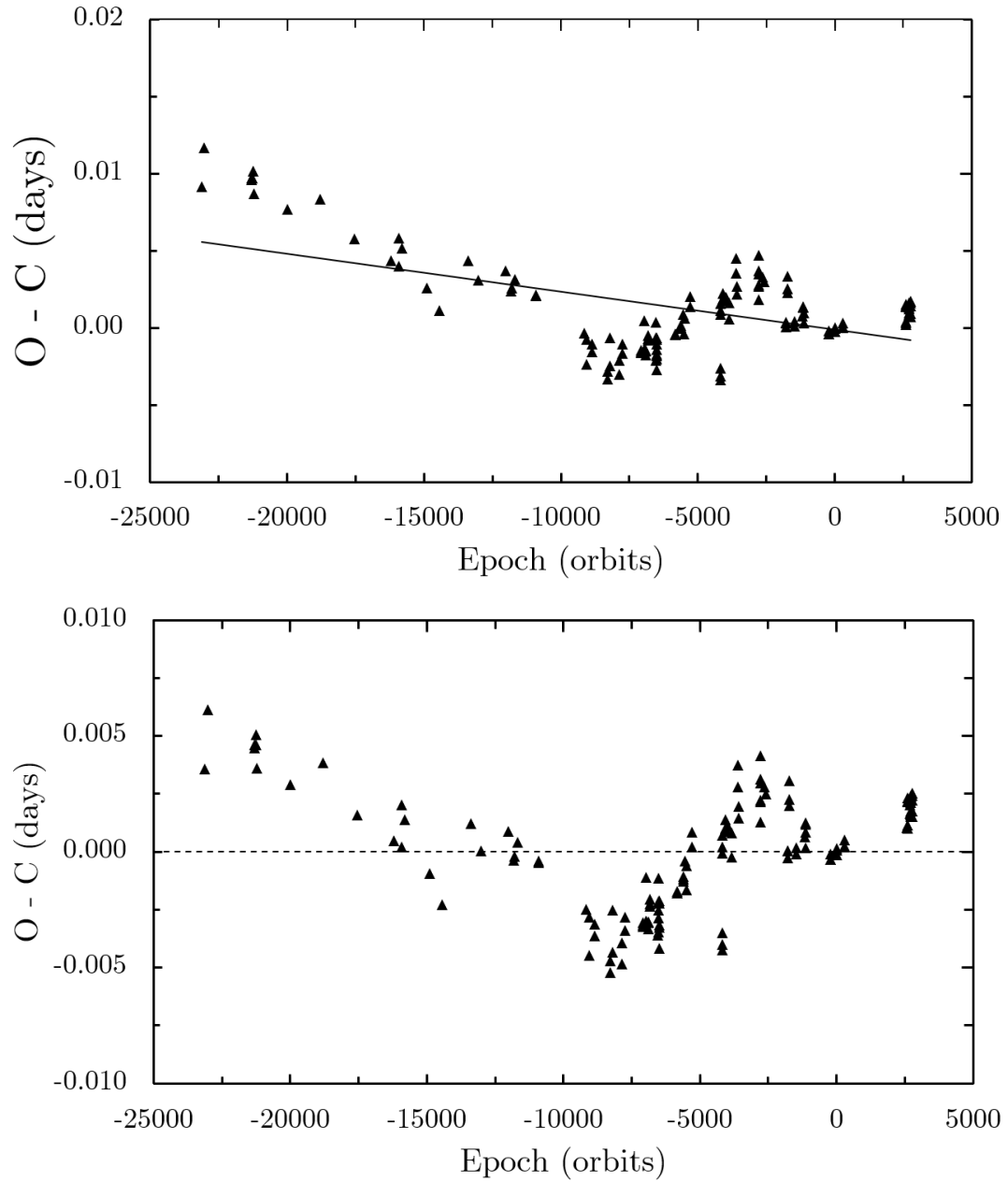
Figure 5.1: *Top:* O-C residuals from Equation 5.1 with the linear ephemeris fit of Equation 5.2. *Bottom:* O-C residuals of the linear regression.
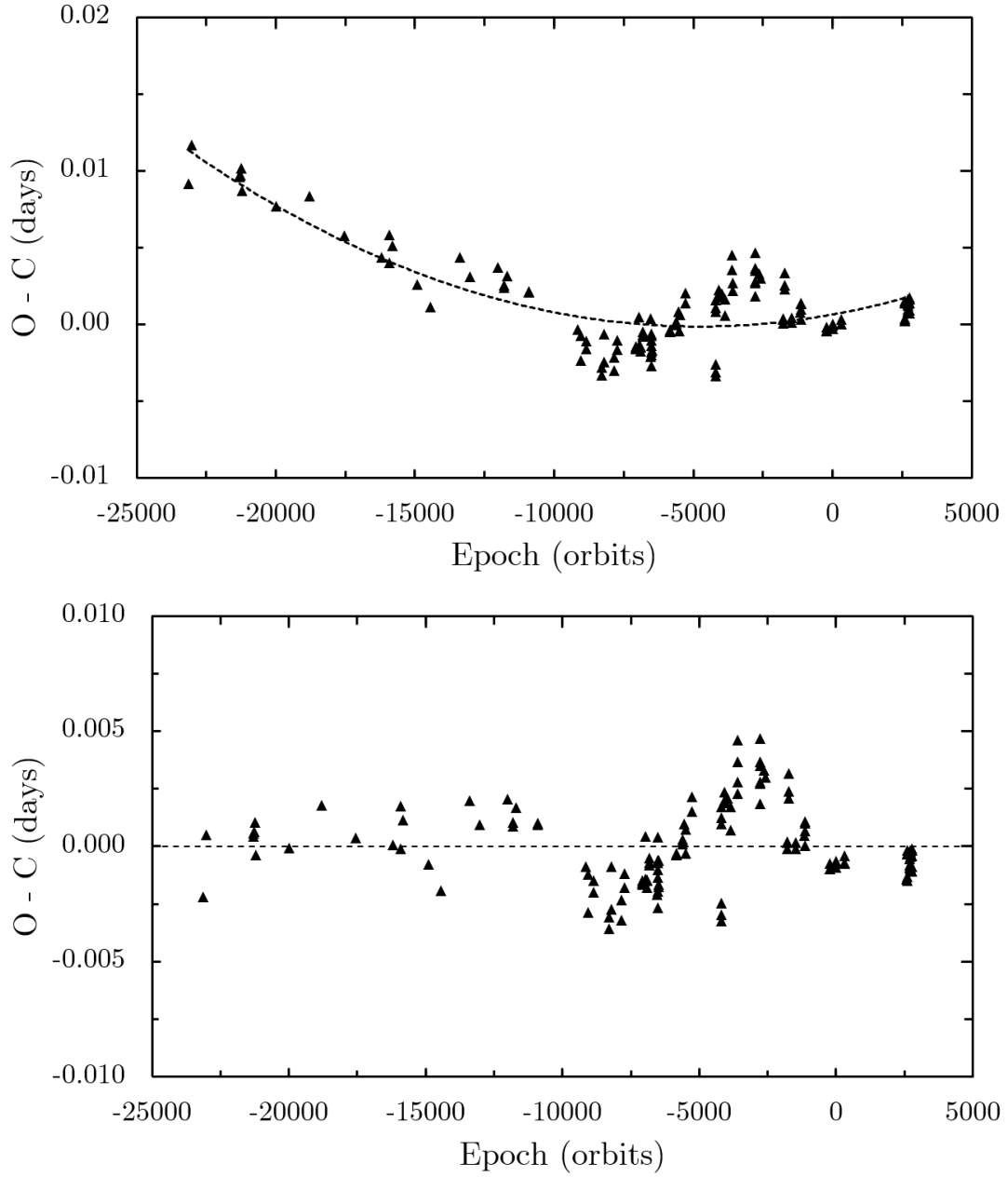
Figure 5.2: *Top:* O-C residuals from Equation 5.1 with the solid line the quadratic fit of Equation 5.4. *Bottom:* O-C residuals of the quadratic regression.

CHAPTER 6

Photometric Light Curve Analysis

<u>Wilson-Devinney Program</u>

The Wilson-Devinney (WD) program is a differential corrections method used to determine the stellar and orbital parameters of a binary star system (Wilson and Devinney 1971). It uses the Roche model to calculate synthetic light curves and attempts to minimize the residuals of the observed minus calculated light curves. The program takes as its input a set of initial parameters and the folded, normalized observational light curves and outputs the suggested parameter corrections, correlation coefficients, new values, and sum of the squares of the residuals. More than one parameter can be corrected at a time provided the correlation coefficients are low. Wilson-Devinney solutions involve a multi-parameter solution space with many local minima which makes it easy to skip over from one minima to another; this can be avoided by carefully monitoring the residuals such that corrections are only implemented when they decrease the residuals. However, finding the best solution can still be quite difficult due to the existence of so many local minima. The resulting solution is determined in large part by what initial estimates are used for the physical parameters.

Binary Maker 3 Program

An initial attempt to visually fit the light curve with Binary Maker 3 can be very helpful in determining a initial estimate that is much more likely to result in the best solution. The Binary Maker 3 (BM3) software also uses the Roche model to generate a three-dimensional model and synthetic light curve from a set of physical parameters specified by the user (Bradstreet 2005). Unlike the WD program, BM3 makes no attempt to correct parameter input. However, it does offer the option to display the observational light curve overlayed by the synthetic light curve, a residual graph, and a 3D animation of the rotating stars. As such, BM3 is extremely useful in developing an intuitive understanding of the physical parameters of a binary system their corresponding light curve features.

Photometric Solutions for V574 Lyr

Light curves from individual observing runs were plotted as a function of phase and were combined with data from observing runs of the same filters to create g', r', and i' folded light curves (Figure 4.1). The data within each light curve were then binned by 0.01 phase increments. Since the maximum magnitude occurred at 0.75 phase in all three filters, each binned light curve was normalized with respect to this value to create normalized flux plots. These data were saved as tab delimited files for g', r', and i' data and were imported into BM3 for use in determining a set of physical parameters with which to start a WD solution.

A rough estimate was made with which to start visually fitting the light curves

in BM3. A total eclipse with an orbital inclination of 90° would be indicated by a primary eclipse with a flat minima. The observed light curves did not demonstrate this characteristic, indicating an inclination less than 90°. The initial estimate was set at 85°. The mass ratio $M_2/M_1 = 2$ of the system was estimated from equations 6.1 and 6.2 from the work of Gazias and Stepien (2008).

$$M_2 = (0.755 \pm 0.059) \log P + (0.416 \pm 0.024) \tag{6.1}$$

$$M_1 = (0.352 \pm 0.166) \log P - (0.262 \pm 0.067) \tag{6.2}$$

The effective temperature of the primary star was estimated using color index. First the extinction in the visual range and the color excess from 3D dust mapping from Pan-STARRS 1 were determined using the galactic coordinates of V574 Lyr (Green, *et al.* 2018). This was arguably a small correction given that the distance to V574 Lyr is 225 ± 1 parsecs but it was included for thoroughness (Gaia Collab. 2016). The average observed g'-r' magnitude (Figure 6.1) was then converted to an average B-V value using the transformation equation shown in equation 6.3 from Jester, *et al.* (2005). This value was then adjusted by the extinction determined from the dust map. Finally, the table of B-V values and corresponding effective temperatures were interpolated from the tables of Pecault and Mamajek (2013). The effective temperature of the primary star was assigned the value 5080 ± 105 K.

$$(B - V) = 0.98 (g - r) + 0.22 \tag{6.3}$$

From inspection of the normalized light curves, the temperature of the secondary
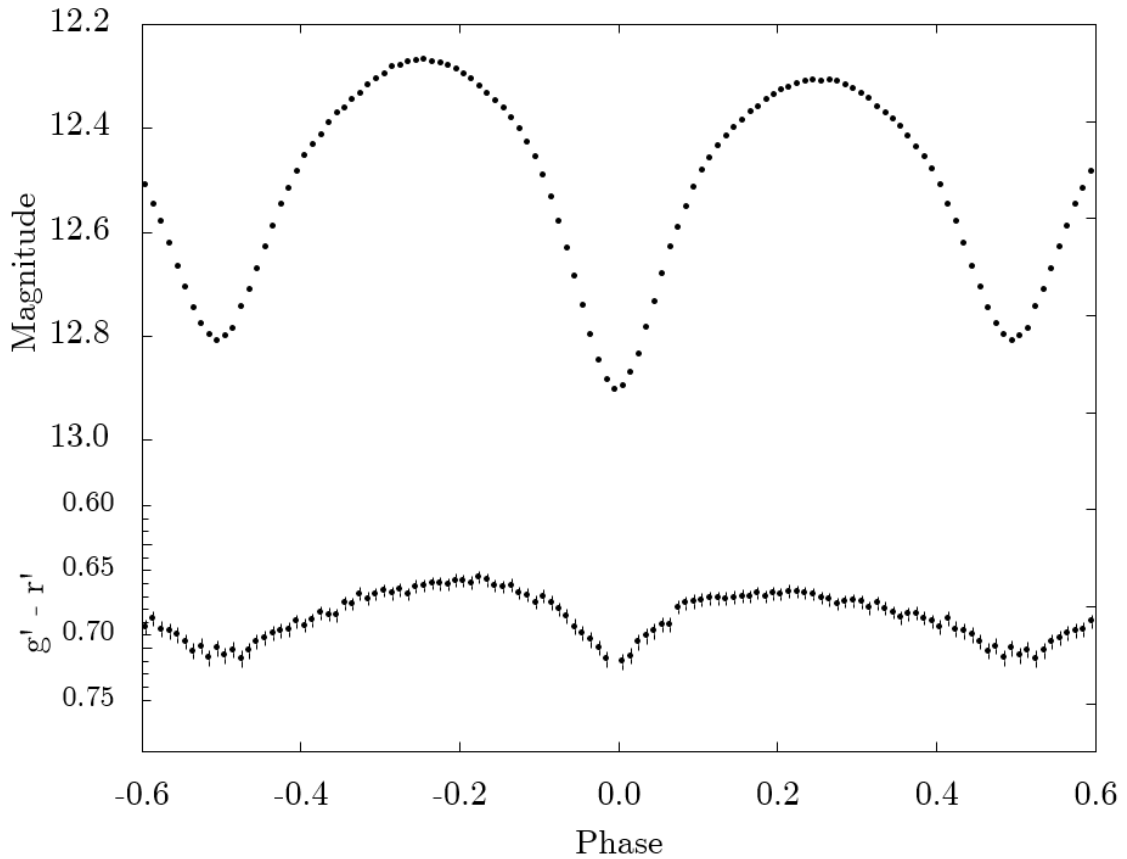
Figure 6.1: Above: Sloan g' binned light curve plotted versus phase. Below: Sloan g'-r' magnitude versus phase.

star was estimated to be a few hundred Kelvin less than the primary. The secondary star was assigned an initial temperature of $T_2 = 4800$ K. Fillouts for contact binaries are typically between 0.1 and 0.2. A fillout of 0.2 was assigned and BM3 was used to calculate the modified potentials from this value. These were $\Omega_1 = \Omega_2 = 5.132$. Bolumetric albedo for both stars was assigned the value of 0.5 for convective stars (Rucinski 1969). Gravity brightening coefficients were set at 0.32 per the work of Lucy (1967). Limb darkening coefficients were computed by the WD program based on temper-

ature estimates, metallicity, and surface gravity for each star (Van Hamme 1993). Additionally, the eccentricity of the orbit was assigned the value $e = 0$ since tidal interaction of contact binaries is very effective at circularization and synchronization of orbits and rotation. For simplicity, spots were left out of the first simulations although the presence of different height maxima at quadrature is a good indication of star spots. The initial estimate of parameters for BM3 are summarized in Table 6.1.

Table 6.1: Initial stellar parameter values for BM3.

Parameter:	Symbol:	Value
Orbital Inclination	i (°)	85
Mass Ratio	q (M_2/M_1)	2.0
Temperature	T_1 (K)	5080
	T_2 (K)	4800
Modified Potentials	$\Omega_1 = \Omega_2$	5.132
Fillout		0.20
Gravity Brightening	G_1	0.32
	G_2	0.32
Limb Darkening	X_1	0.859
(Sloan g')	X_2	0.842
Limb Darkening	X_1	0.700
(Sloan r')	X_2	0.784
Limb Darkening	X_1	0.586
(Sloan i')	X_2	0.701
Bolumetric Albedo	Star 1	0.5
	Star 2	0.5

Orbital inclination, mass ratio, secondary temperature, and omega potentials were manually adjusted over repeated simulations to visually fit the observed normalized light curve and minimize the residuals until it became apparent that no better fit would be found without the addition of spots. The synthetic and observed light curves in the g' filter are shown in Figure 6.2 and the parameters for this no-spot

model are summarized in Table 6.2 with the gravity brightening coefficient, limb darkening coefficients, and albedos remaining unchanged from the initial input values.

Table 6.2: Stellar parameters for the BM3 model without spots.

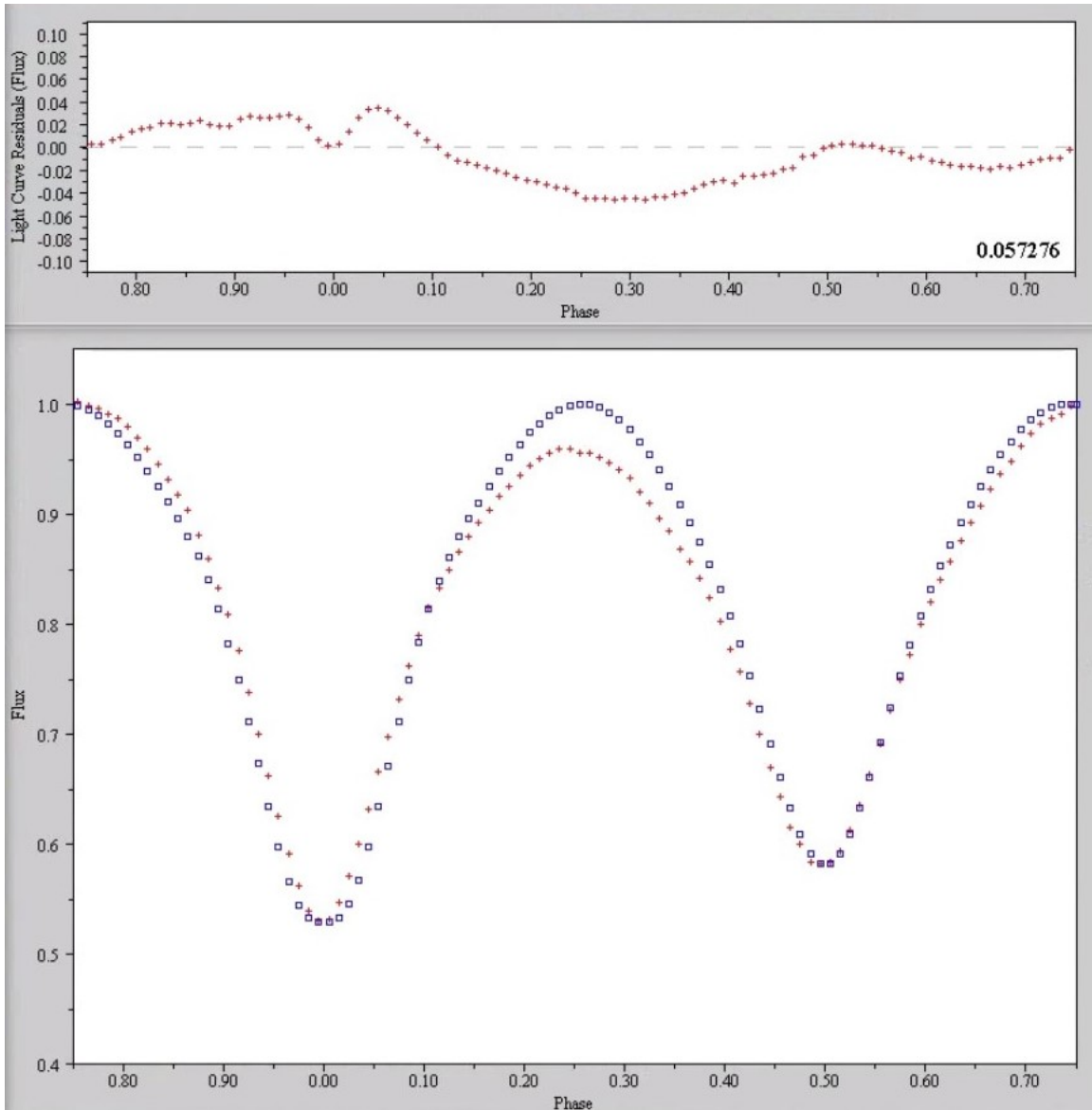| Star Parameter:	Symbol:	Value
Orbital Inclination	i (°)	79.7
Mass Ratio	q (M_2/M_1)	2.9
Temperature	T_1 (K)	5080
	T_2 (K)	4800
Modified Potentials	$\Omega_1 = \Omega_2$	6.366
Fillout		0.19

Figure 6.2: A screen shot of the BM3 model fit using parameters from Table 6.2. The synthetic (blue □) and observed (red +) light curves are shown below and the residuals above.

Subsequently, cool spots were added to the primary star and were adjusted until reasonably close synthetic light curves were achieved in all three filters (see Figure 6.3 for Sloan g'). The resulting parameters summarized in Table 6.3 were then used to begin the Wilson-Devinney solution.

Table 6.3: An adjusted estimate of stellar parameters with spots from Binary Maker 3.

Stellar Parameter:	Symbol:	Value
Orbital Inclination	i (°)	78.0
Mass Ratio	q (M_2/M_1)	2.85
Temperature	T_1 (K)	5080
	T_2 (K)	4770
Modified Potentials	$\Omega_1 = \Omega_2$	6.400
Fillout		0.028
Spot 1, Star 1	Colatitude (°)	61.0
	Longitude (°)	83.0
	Radius (°)	19.0
	Temperature Factor	0.880
Spot 2, Star 1	Colatitude (°)	51.0
	Longitude (°)	343
	Radius (°)	14.8
	Temperature Factor	0.834

The WD program was configured to mode 3 for a contact binary system (modified potentials are constrained to be equivalent for both stars since they share a convective envelope). An input file was created with the parameters from the spot model of BM3 and the solution proceeded with sets of parameters being corrected until the residuals reached a minimum. The results of the WD solution *without* spots are summarized in Table 6.4 and the synthetic light curves overlaying the observed light curves are shown in Figure 6.4. It was found that no third light is present in this system. Note that while the residuals of this solution have been minimized, the resulting synthetic

light curves show less than desired agreement with the observed light curves, notably in the phase ranges $0.2 - 0.4$ and $0.7 - 0.9$. Dark spots on the stellar surfaces are the most likely cause of the poor fit.

Table 6.4: Stellar paramteres from the WD model without spots.

Star Parameter:	Symbol:	Value:	
Orbital Inclination	i (°)	76.058	±2
Mass Ratio	q (M_2/M_1)	2.92041	±0.05
Temperature	T_1 (K)	5080	
	T_2 (K)	4757	±15
Omega Potentials	$\Omega_1 = \Omega_2$	6.3826	±0.07
Fillout		0.2074	
Lights	L_1	4.4	±0.2
(Sloan g')	$L_1/(L_1 + L_2)$	0.38	±0.02
Lights	L_1	4.1	±0.2
(Sloan r')	$L_1/(L_1 + L_2)$	0.35	±0.02
Lights	L_1	4.0	±0.2
(Sloan i')	$L_1/(L_1 + L_2)$	0.34	±0.02
Residuals:	Σw^2	0.0028530	

A similar process was used to find a solution with spots. The star parameter sets were first corrected until the residuals reached a minimum and then spot parameter sets were corrected. The process was repeated until no further corrections could be made without increasing the residuals. The results of the WD solution *with* spots are summarized in Table 6.5. Again, no third light was found to be part of this system. Notice that the residuals of the WD spot solution are significantly lower than those of the WD no-spot model (see Table 6.4). Visually, the synthetic light curves in Figure 6.5 show good agreement with the observed light curves. The primary minima in the r' filter and the secondary minima in the g' filter show more light than observed, but this could be due to spot drifting over the two month period of observation; this

hypothesis is supported by the large error of the spot colatitudes and longitudes. The i' synthetic and observed light curves show excellent agreement.

Table 6.5: Stellar parameters from the WD model with spots.

Star Parameter:	Symbol:	Value:	
Orbital Inclination	i (°)	76.911	±0.6
Mass Ratio	q (M_2/M_1)	2.89879	±0.02
Temperature	T_1 (K)	5080	±105
	T_2 (K)	4766	±14
Modified Potentials	$\Omega_1 = \Omega_2$	6.39313	±0.03
Fillout		0.1439	
Lights	L_1	4.47	±0.06
(Sloan g')	$L_1/(L_1 + L_2)$	0.376	±0.005
Lights	L_1	4.15	±0.06
(Sloan r')	$L_1/(L_1 + L_2)$	0.347	±0.005
Lights	L_1	4.04	±0.06
(Sloan i')	$L_1/(L_1 + L_2)$	0.335	±0.005
Spot 1, Star 2	Colatitude (°)	61.13	±12
	Longitude (°)	79.37	±5.5
	Radius (°)	19.00	±2.4
	Temperature Factor	0.8748	±0.029
Spot 2, Star 2	Colatitude (°)	51.19	±22
	Longitude (°)	337.61	±15
	Radius (°)	14.29	±4.2
	Temperature Factor	0.8290	±0.052
Residuals	Σw^2	0.000823324	

Since the WD solution space does contain many local minima, at a later date it would be recommended to complete a q-search (completing WD solutions across a grid of fixed mass ratios) to determine the mass ratio corresponding to the absolute minimum of residuals. The resulting mass ratio from a q-search could then incorporated into a new WD solution attempt.
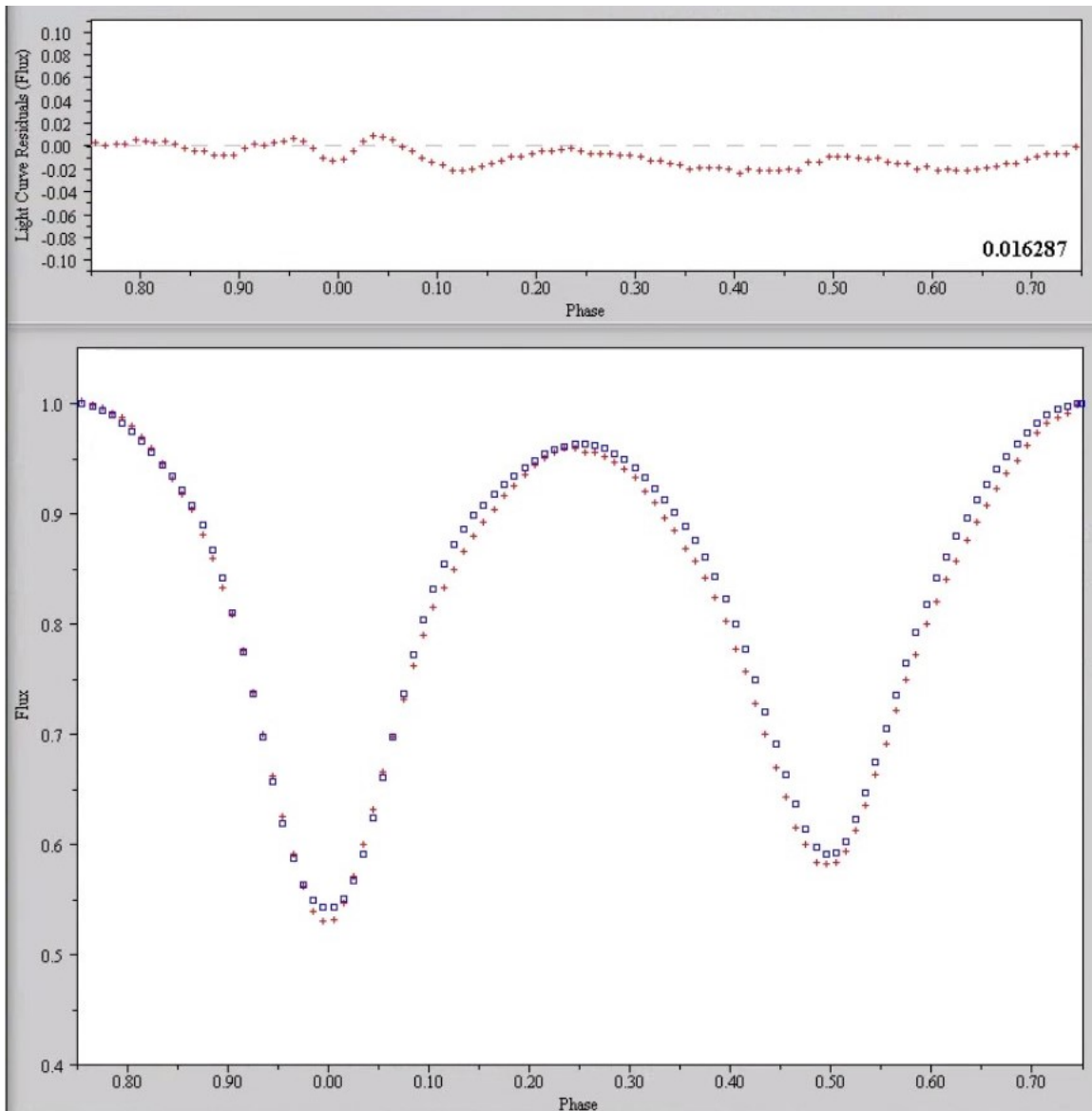
Figure 6.3: A screen shot of the BM3 model fit using parameters from Table 6.3. The synthetic (blue □) and observed (red +) light curves are shown below and the residuals above.
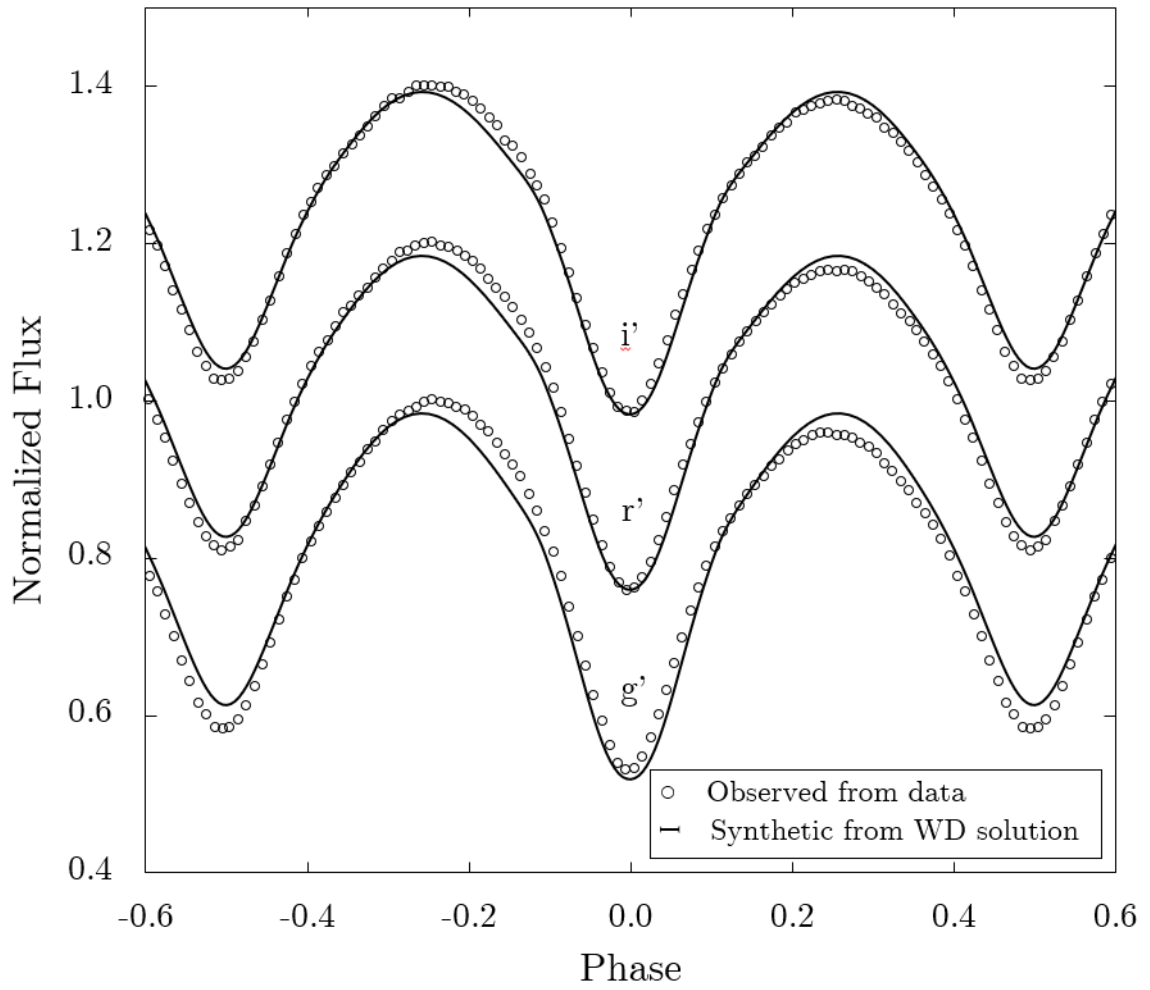
Figure 6.4: Synthetic and observed light curves for the WD solution without spots.
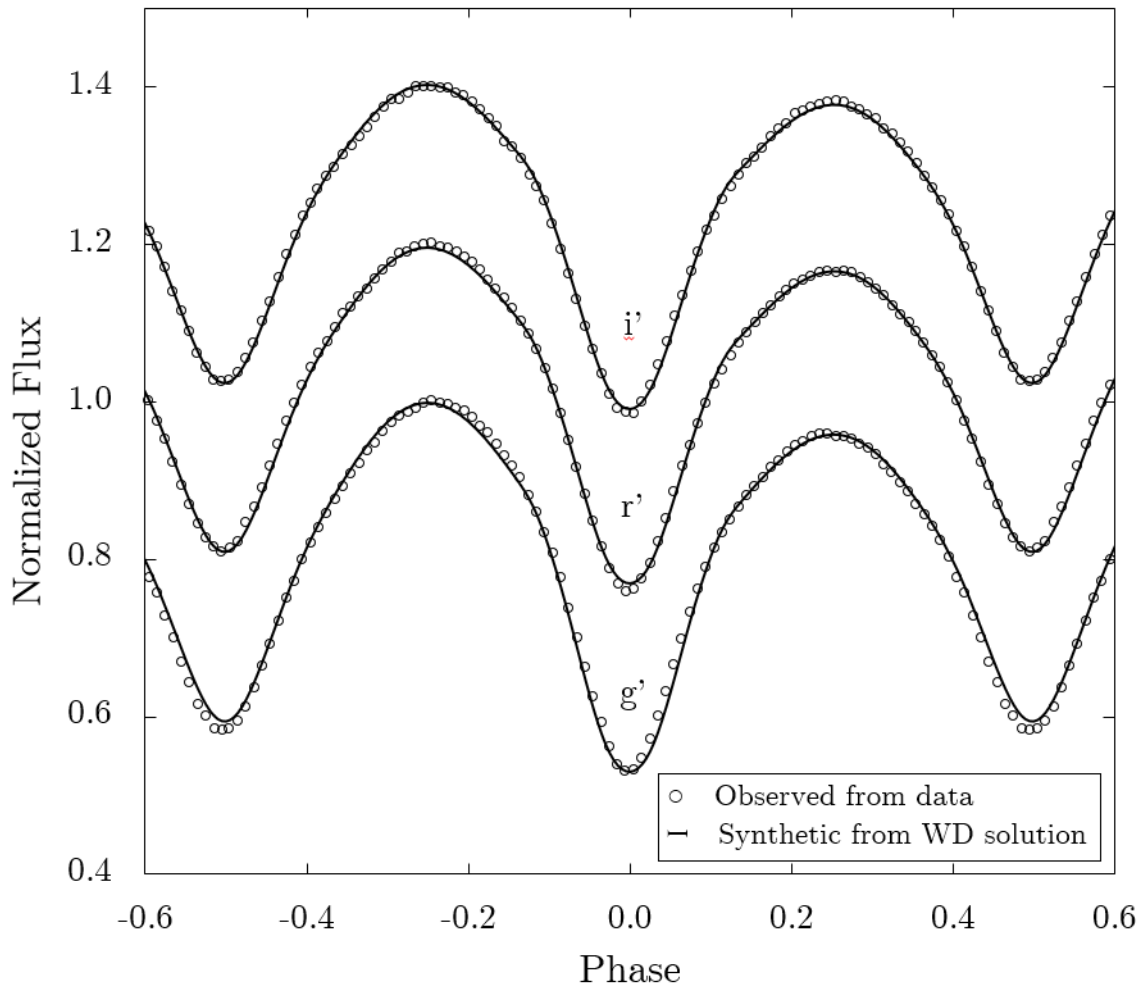
Figure 6.5: Synthetic and observed light curves for the WD solution with spots.

CHAPTER 7

Conclusions

<u>Analysis</u>

The final WD parameters from the with-spot solution were used to model V574 Lyr. The final model produced by Binary Maker 3 shown in Figure 7.1 shows the primary star with two cool spots, the larger of which is nearly facing the observer at the first quadrature (0.25 phase). In actuality, the star may not have only two large cool spots, but instead several smaller cooler spots from magnetic activity localized in two specific regions on the primary star. These two large spots would then approximate the possible many smaller spots.

Figure 7.1: Roche lobe surfaces of the best-fit WD spot model. The binary is shown starting at 0.75 phase in 0.11 phase increments.

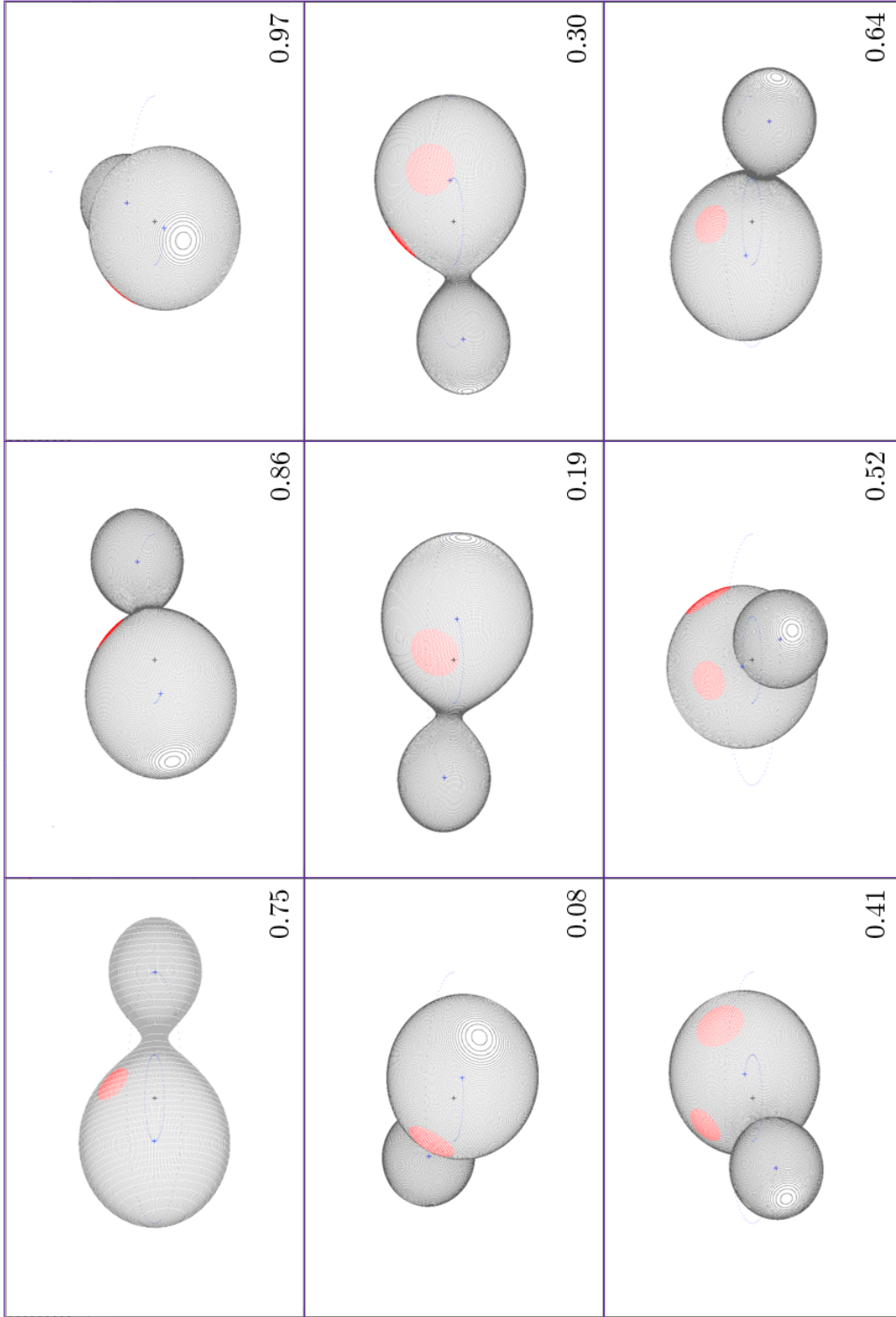Many factors point to V574 Lyr being a W-type as opposed to an A-type W UMa binary system. Reviewing Binnendijk's (1965) and Rucinski's work (1973 and 1974) we see that a W-type W UMa system generally exhibits the following features:

1. The primary minima are caused by an eclipse of the smaller secondary star by the larger primary star.

2. Surface temperatures of the stars are equal to or less than 6000 K to 6200 K.

3. Mass ratios (M_2/M_1) are typically between 1.1 and 3.0.

4. The orbital period is changing.

5. The mass transfer between stars is typically on the order of 10^{-7} solar masses per year.

It can be seen from Figure 7.1 that the primary minimum occurring at zero phase is indeed caused by the partial eclipse of the smaller secondary star. Additionally, from the solution of V574 Lyr in Table 6.5 we see that the surface temperatures and mass ratio are within the range of values typical of W-type system. It was noted previously from the period study that the orbital period of the system is changing. Mass transfer rate can be calculated using the equation:

$$\frac{dM}{dt} = \frac{PM_1M_2}{3P\left(M_1 - M_2\right)} \tag{7.1}$$

Using the quadratic ephemeris and estimates of masses (Table 7.1) from the mass ratio and the work of Gazeas and Stepien (2008) it is found that there is a possible mass transfer rate of 10^{-7} solar masses per year between the stars. Since the period of

the system is increasing and assuming conservative mass transfer, the more massive star, M_2, should be gaining mass while the less massive star, M_1 is losing mass. Both the mass transfer rate and changes in period are again typical of W-type systems.

Table 7.1: Estimated absolute parameters for V574 Lyr. Starred values are provisional; radial velocity data is need to confirm these values.

Parameter:	Symbol:	Value:	
Stellar Mass*	M_1 ($M_\odot$)	0.338	± 0.032
	M_2 ($M_\odot$)	0.978	± 0.092
Semi-major Axis*	a ($R_\odot$)	1.94	± 0.05
Mean Stellar Radii	R_1 ($R_\odot$)	0.583	± 0.014
	R_2 ($R_\odot$)	0.939	± 0.023
Stellar Luminosity	L_1 ($L_\odot$)	0.204	± 0.022
	L_2 ($L_\odot$)	0.410	± 0.051
Bolometric Magnitude	$M_{1(bol)}$	6.5	± 0.1
	$M_{2(bol)}$	5.7	± 0.1
Surface Gravity	$\log g_1$ ($\log g_\odot$)	4.43	± 0.04
	$\log g_2$ ($\log g_\odot$)	4.48	± 0.04
Mean Density	ρ_1 ($\rho_\odot$)	2.40	± 0.06
	ρ_2 ($\rho_\odot$)	1.66	± 0.08

From the period study, the quadratic O-C residuals show evidence of some higher order polynomial or sinusoidal trend. This could suggest the presence of a third body in the system. The lack of third light in the WD solution indicates that if a third body is present it contributes a negligible amount of light to the system due to small size relative to the two main components, large distance from the two main components, or both.

Luminosities were calculated from the star masses and effective radii given by the light curve routine with the Wilson-Devinney program (Table 7.1). From the temperatures and luminosities we can infer that the components are mostly likely late type (spectral class G - M) main sequence stars. The total luminosity of the system

from the WD solution is $L = 0.61 \pm 0.07$ and agrees with the observed luminosity of 0.52 ± 0.03 within the errors.

Summary

A WD photometric solution of V574 Lyr was successfully found. V574 Lyr is a good example of a W-type W UMa eclipsing binary system possessing two spectrally similar main sequence stars. Given several more years of consistent observation, a new period study is suggested to confirm that the period is increasing overall and to elucidate the potential patterns of sudden period change. Perhaps in the future there will be enough data to indicate the presence of a third body in the system. Further work should include completing a q-search to confirm the mass ration presented here. If spectroscopic observations become available, a new WD solution should be attempted using both the radial velocity and photometric observations. The radial velocity observations would provide for the direct determination of the stellar masses and the semi-major axis of the orbit.

This research made use of the SIMBAD, NASA ADS, Vizier, and International Variable Star Index (VSX) databases as well as data from the Gaia mission and the Pan-STARRS1 survey.

REFERENCES

AAVSO. 2014, *The AAVSO Guide to CCD Photometry* AAVSO, Cambridge MA.

AAVSO Photometric All-Sky Survey. (http://www.aavso.org/apass)

AAVSO Variable Star Plotter. (https://www.aavso.org/apps/vsp/)

Akerlof, C., *et al.* 2000, Astron. J., **119**, 1901.

Astrodon FW83-STXL 50 mm filters. (https://farpointastro.com/)

Astronomer's Control Panel. (http://acp.dc3.com/index2.html)

Avvakumova, E.A., and Malkov, O.Y. 2014, Mon. Not. Roy. Astron. Soc., **444**, 1982.

Avvakumova, E.A., Malkov, O.Y., and Kniazev, A.Y. 2013, Astronomische Nachrichten, **334**, 860.

Banfi, M., *et al.* 2012, IAU Inform. Bull. Var. Stars, **6033**, 1.

Binary Maker 3. (www.binarymaker.com)

Binnendijk, L. 1965, Kl. Veroeffentl. Remeis-Sternw. Bamberg, **4**, 36.

Blättler, E., and Diethelm, R. 2000, IAU Inform. Bull. Var. Stars, **4976**, 4.

Blättler, E., *et al.* 2000, BBSAG Bull., **123**, 1.

Blättler, E., *et al.* 2001, BBSAG Bull., **126**, 1.

Blättler, E., *et al.* 2002, BBSAG Bull., **128**, 1.

Bradstreet, D.H. 2005, in *Society for Astronomical Sciences, 24th Annual Symposium*, Society for Astronomical Sciences, Rancho Cucamonga, CA, 23.

Brat, L., *et al.* 2011, Open European Journal on Variable Stars, **137**, 1.

Brat, L., Zejda, M., and Svoboda, P. 2007, Open European Journal on Variable Stars, **74**, 1.

Bruton, D. 2018, "Heliocentric Julian Day",
(http://www.physics.sfasu.edu/astro/javascript/hjd.html).

Coughlin, J.L., *et al.* 2014, Astron. J., **147**, 119.

Davis Weather Station. (https://www.davisinstruments.com/).

Diethelm, R. 2003, IAU Inform. Bull. Var. Stars, **5438**, 1.

Diethelm, R. 2004, IAU Inform. Bull. Var. Stars, **5543**, 1.

Diethelm, R. 2006, IAU Inform. Bull. Var. Stars, **5713**, 1-8.

Diethelm, R. 2006, IAU Inform. Bull. Var. Stars, **5781**, 1-6.

Diethelm, R. 2008, IAU Inform. Bull. Var. Stars, **5837**, 1.

Diethelm, R. 2010, IAU Inform. Bull. Var. Stars, **5920**, 1.

Diethelm, R. 2010, IAU Inform. Bull. Var. Stars, **5945**, 1.

Diethelm, R. 2012, IAU Inform. Bull. Var. Stars, **6029**, 1.

Drake, A.J., *et al.* 2013, Astrophys. J., **763**, 32.

Flexible Image Transport System. (https://fits.gsfc.nasa.gov/fits_home.html).

FocusMax 4.0. (https://www.focusmax.org/).

Gaia Collaboration 2016, Astron. and Astrophys., **595**, A1.

Gazeas, K., and Stepien, K. 2008, Mon. Not. Roy. Astron. Soc., **390**, 1577.

Gettel, S.J., Geske, M.T., and McKay, T.A. 2006, Astron. J., **131**, 621.

Green, G.M., *et al.* 2018, Mon. Not. Roy. Astron. Soc., **478**, 651.

Hoffman, D.I., Harrison, T.E., and McNamara, B.J. 2009, Astron. J., **138**, 466.

Honkova, K., *et al.* 2013, Open European Journal on Variable Stars, **160**, 1.

Honkova, K., *et al.* 2014, Open European Journal on Variable Stars, **165**, 1.

Honkova, K., *et al.* 2015, Open European Journal on Variable Stars, **168**, 1.

Howell, S.B. 2006, *Handbook of CCD Astronomy*, Cambridge Univ. Press, Cambridge, UK.

Hubscher, J. 2007, IAU Inform. Bull. Var. Stars, **5802**, 1.

Hubscher, J. 2013, IAU Inform. Bull. Var. Stars, **6084**, 1.

Hubscher, J. 2016, IAU Inform. Bull. Var. Stars, **6157**, 1.

Hubscher, J., Braune, W., and Lehmann, P.B. 2013, IAU Inform. Bull. Var. Stars, **6048**, 1.

Hubscher, J., Lehmann, P.B., and Walter, F. 2012, IAU Inform. Bull. Var. Stars, **6010**, 1.

Hubscher, J., and Lehmann, P.B. 2013, IAU Inform. Bull. Var. Stars, **6070**, 1.

Hubscher, J., and Lehmann, P.B. 2015, IAU Inform. Bull. Var. Stars, **6149**, 1.

Hubscher, J., Paschke, A., and Walter, F. 2005, IAU Inform. Bull. Var. Stars, **5657**, 1.

Hubscher, J., Paschke, A., and Walter, F. 2006, IAU Inform. Bull. Var. Stars, **5731**, 1-31.

Hubscher, J., Steinbach, H.M., and Walter, F. 2009, IAU Inform. Bull. Var. Stars, **5874**, 1.

Jester, S. *et al.* 2005, Astron. J.,**130**, 873.

Jurysek, J., *et al.* 2017, Open European Journal on Variable Stars, **179**, 1.

Kallrath, J., and Milone, E.F. 1999, *Eclipsing Binary Stars*, Spring-Verlag New York, Inc., New York, NY.

Kazarovets, E.V., *et al.* 2003, Inform. Bull. Var. Stars, **5422**, 1.

Kopal, Z. 1955, Ann. Astrophys., **18**, 379.

Kopal, Z. 1978, *Dynamics of Close Binary Systems*, D. Reidel Publishing Company.

Kreiner, J.M. 2004, Acta Astron., **54**, 207-210.

Lampens, P., *et al.* 2017, Inform. Bull. Var. Stars, **6230**, 1.

Lucy, L.B. 1967, Zeitschrift für Astrophysik, **65**, 89.

Lucy, L.B. 1968, Astrophys. J., **151**, 1123.

Malkov, O.Y., *et al.* 2006, Astron. and Astrophys., **446**, 785.

MaxImDL. (http://diffractionlimited.com/product/maxim-dl/).

Minima v2.4. (https://www.variablestarssouth.org/software-by-bob-nelson/).

Mirametrics. (http://mirametrics.com).

Nelson, R.H. 2008 IAU Inform. Bull. Var. Stars, **5820**, 1.

OPTEC TCF-S3 focuser. (https://www.optecinc.com/).

Pan-STARRS STSci. (https://panstarrs.stsci.edu/).

Pecault, M.J., and Mamajek, E.E. 2013, Astrophys. J. Supp., **208**, 9.

Pribulla, T., Kreiner, J.M., and Tremko, J. 2003, Cont. of the Astron. Obs. Skalnate Pleso, **33**, 38.

Rucinski, S.M. 1969, Acta Astron., **19**, 4.

Rucinski, S.M. 1973, Acta Astron., **23**, 79.

Rucinski, S.M. 1974, Acta Astron., **24**, 119.

SBIG STXL-6303 CCD camera, 2019, (http://diffractionlimited.com/).

SFASU SkyCam. (http://www.observatory.sfasu.edu/).

SkyAlert. 2018, (http://interactiveastronomy.com/index.html).

SkyRoof. 2018, (http://interactiveastronomy.com/index.html).

Software Bisque Paramount MX telescope mount. (http://www.bisque.com/sc/)

Spike-a flat field. (http://www.spike-a.com/flatfielders/).

Sterken, C. 2005, in *The Light-Time Effect in Astrophysics*, ed. C. Sterken, ASP Conf. Ser. **335**, 3.

TheSkyX. (http://www.bisque.com/sc/).

Third Planet Optics. (https://www.tpotelescopes.com/).

Van Hamme, W. 1993, Astron. J., **106**, 2096.

Wilson, R.E., and Devinney, E.J. 1971, Ap. J., **166**, 605.

Observational Light Curves

APPENDIX A

Observational light curves from the thirteen different nights of observation of V574 Lyr during the summer of 2018. Light curves are presented first by filter type (Sloan g', r', and i') and then by date of observation. Gaps in the light curves are from the loss of data due to cloud coverage.
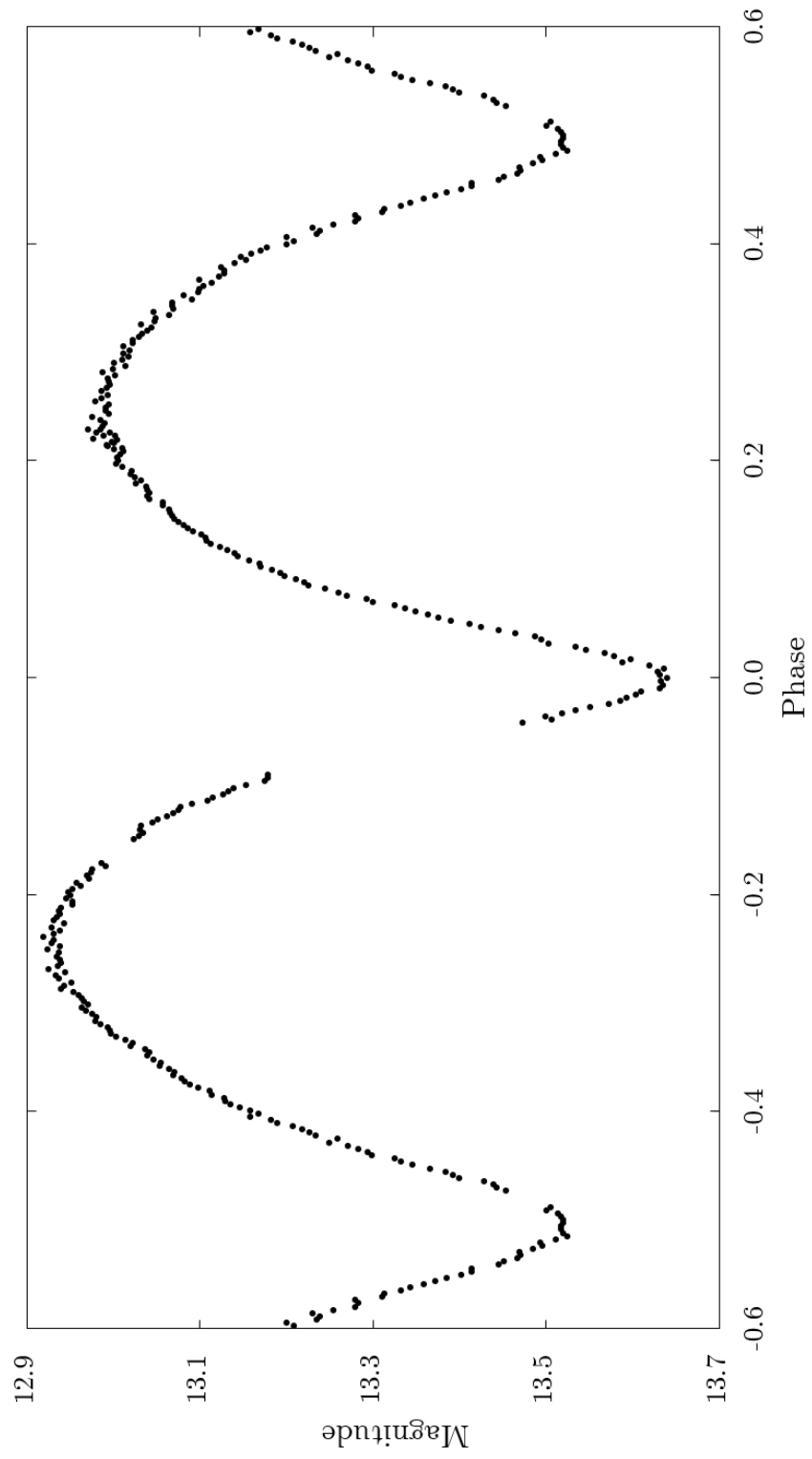
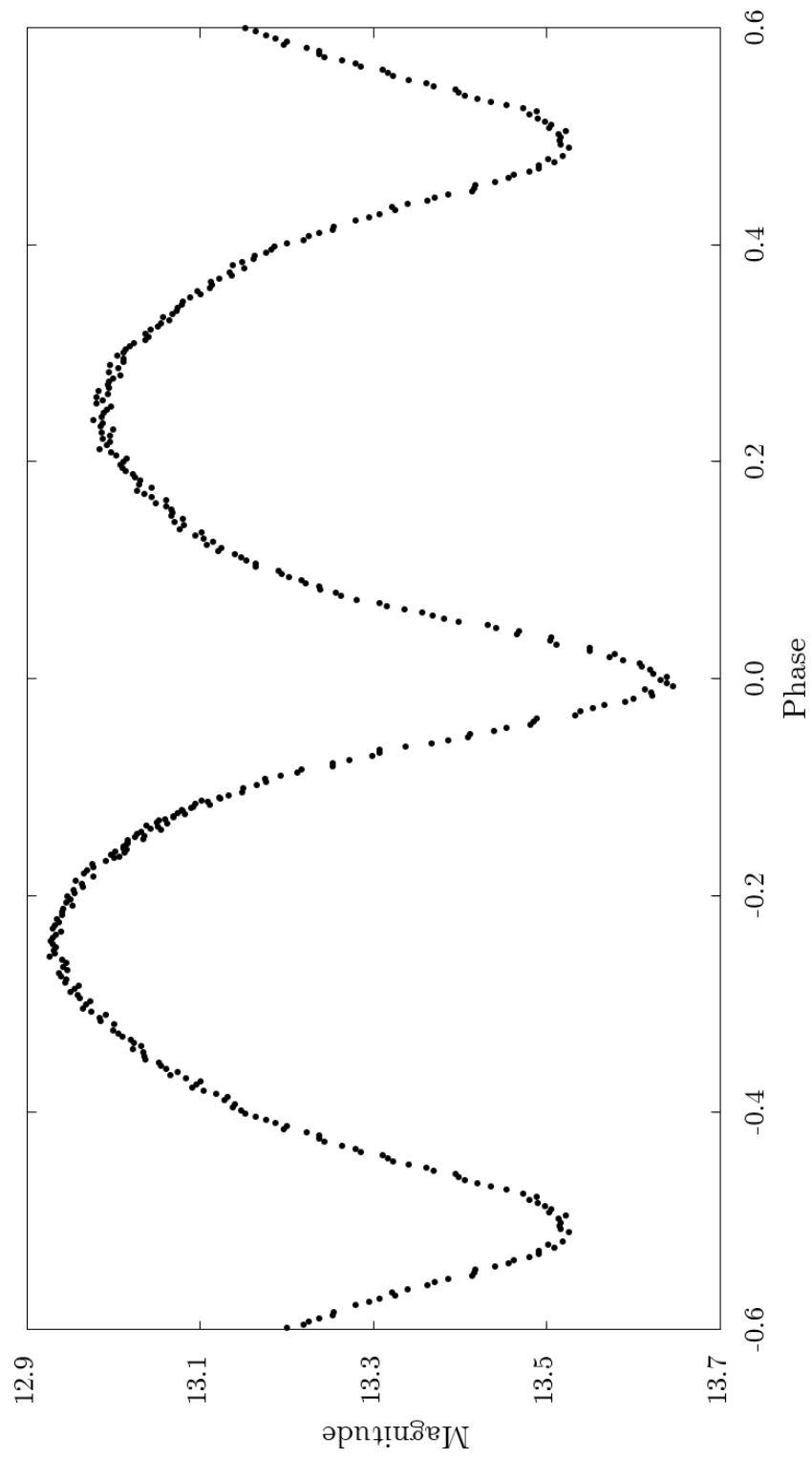Figure A.1: Observational light curve of V574 Lyr from the night of 06/15/18 in the Sloan g' filter.

Figure A.2: Observational light curve of V574 Lyr from the night of 06/16/18 in the Sloan g' filter.

Figure A.3: Observational light curve of V574 Lyr from the night of 07/20/18 in the Sloan g' filter.

Figure A.4: Observational light curve of V574 Lyr from the night of 07/21/18 in the Sloan g' filter.

Figure A.5: Observational light curve of V574 Lyr from the night of 07/31/18 in the Sloan g' filter.
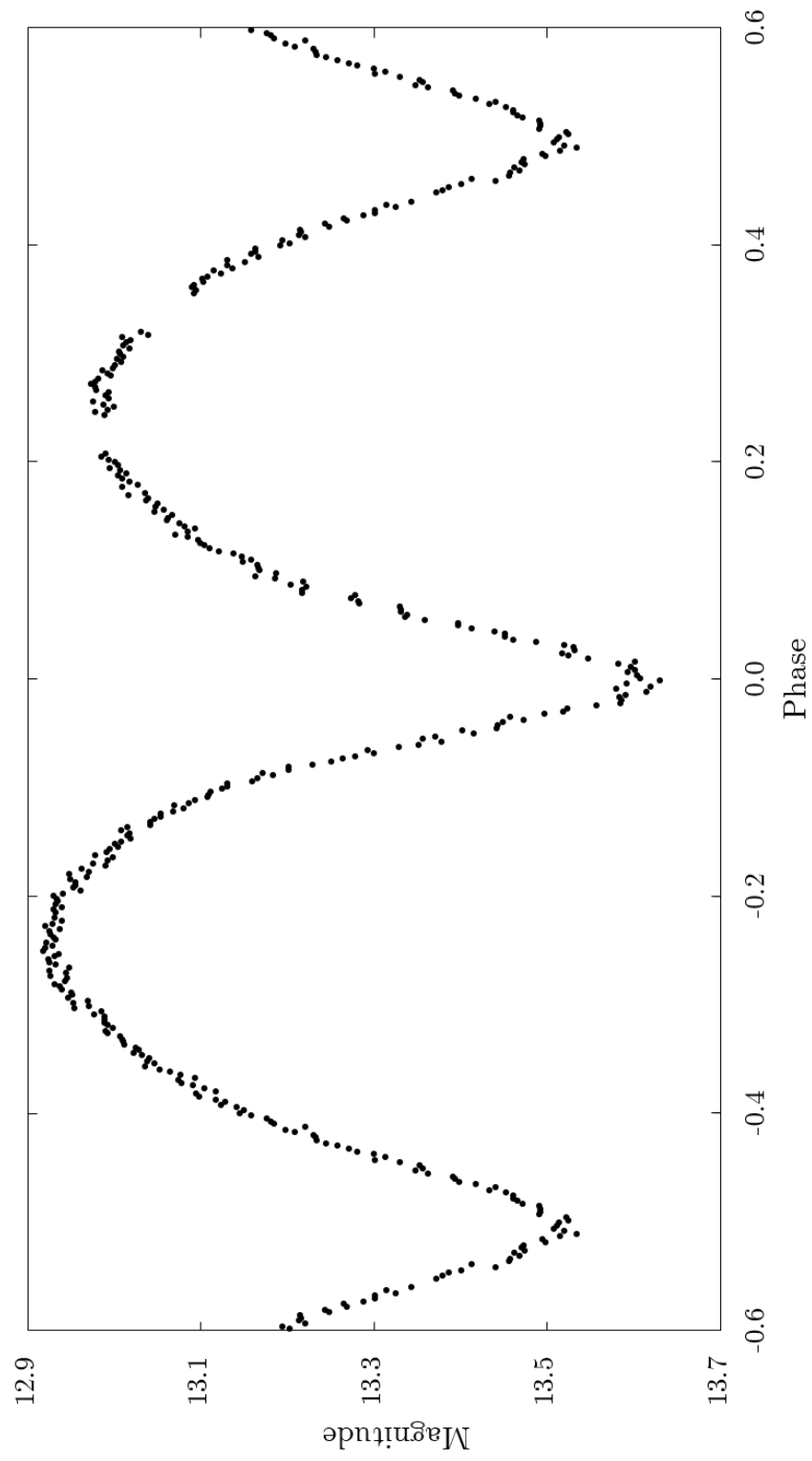
Figure A.6: Observational light curve of V574 Lyr from the night of 08/01/18 in the Sloan g' filter.
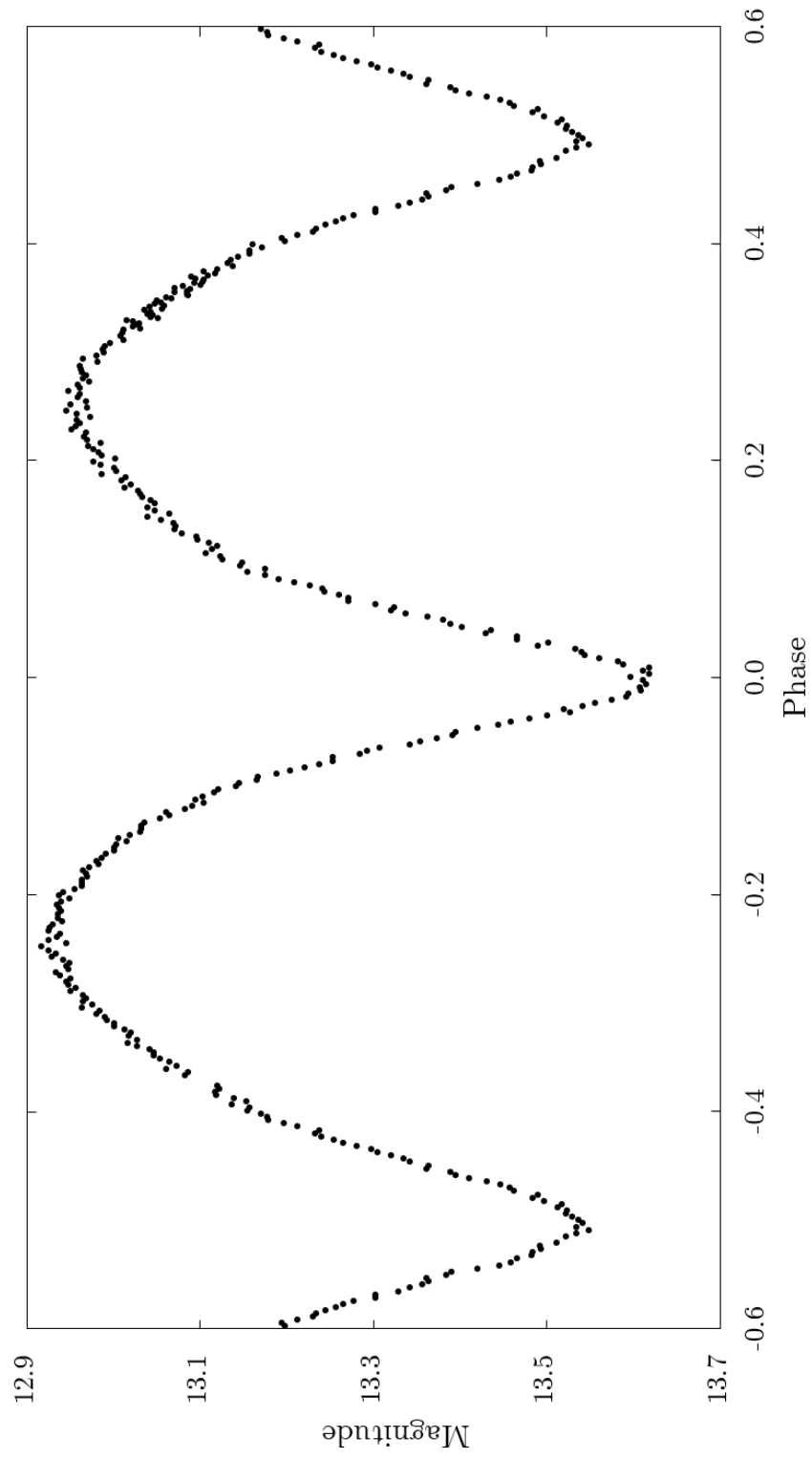
57
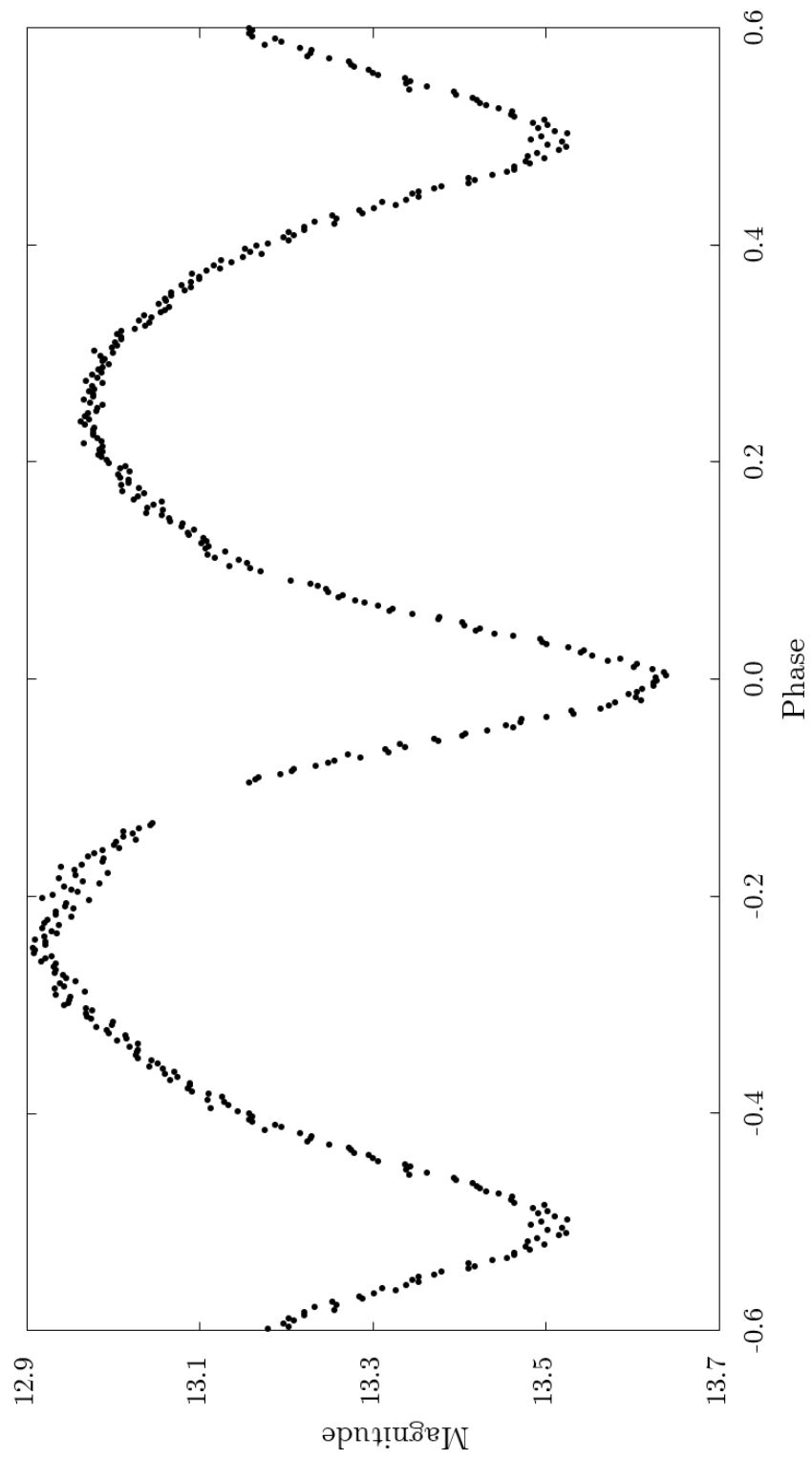
Figure A.7: Observational light curve of V574 Lyr from the night of 08/02/18 in the Sloan g' filter.
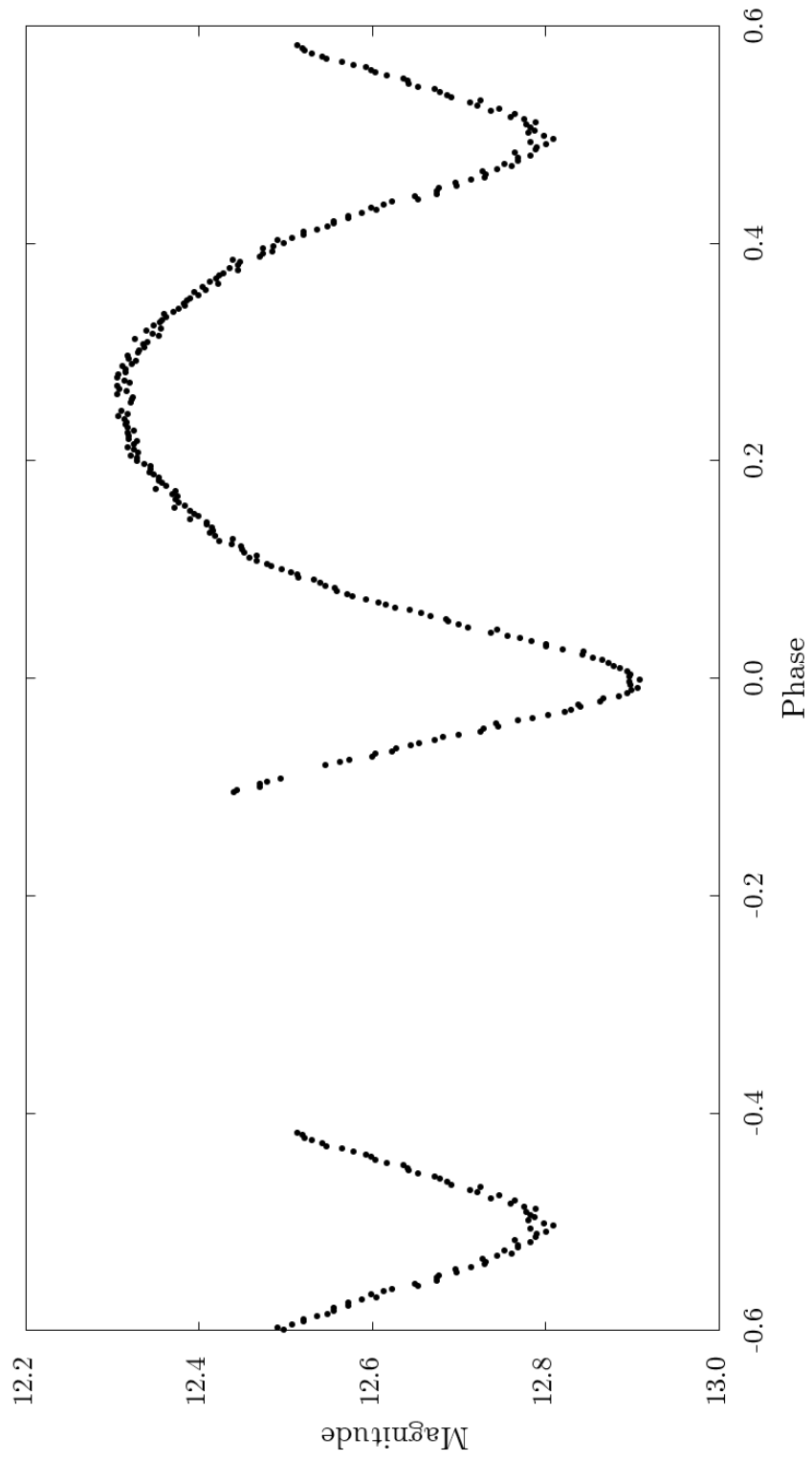
Figure A.8: Observational light curve of V574 Lyr from the night of 06/12/18 in the Sloan r' filter.
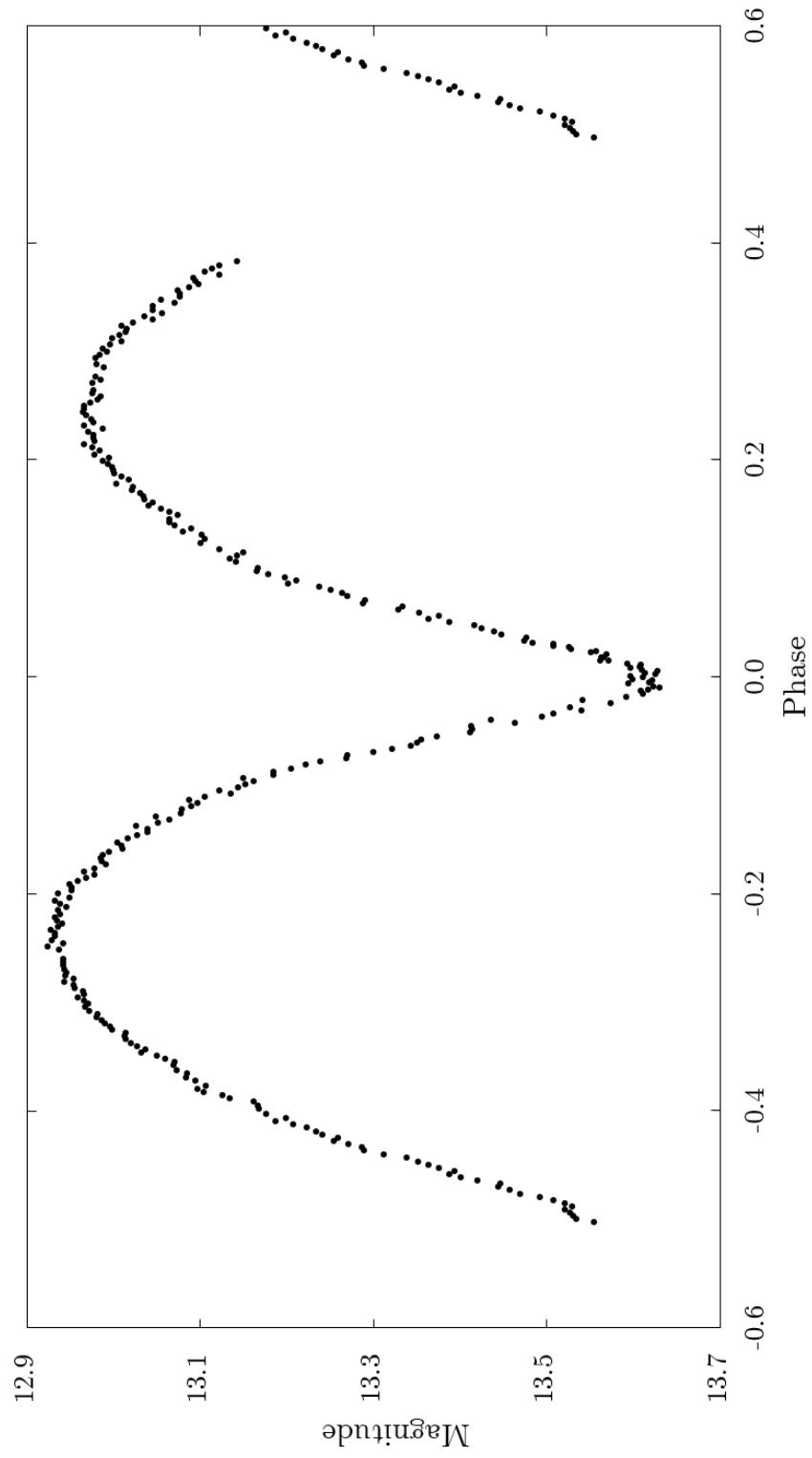
Figure A.9: Observational light curve of V574 Lyr from the night of 06/14/18 in the Sloan r' filter.

Figure A.10: Observational light curve of V574 Lyr from the night of 07/15/18 in the Sloan r' filter.

Figure A.11: Observational light curve of V574 Lyr from the night of 07/19/18 in the Sloan r' filter.
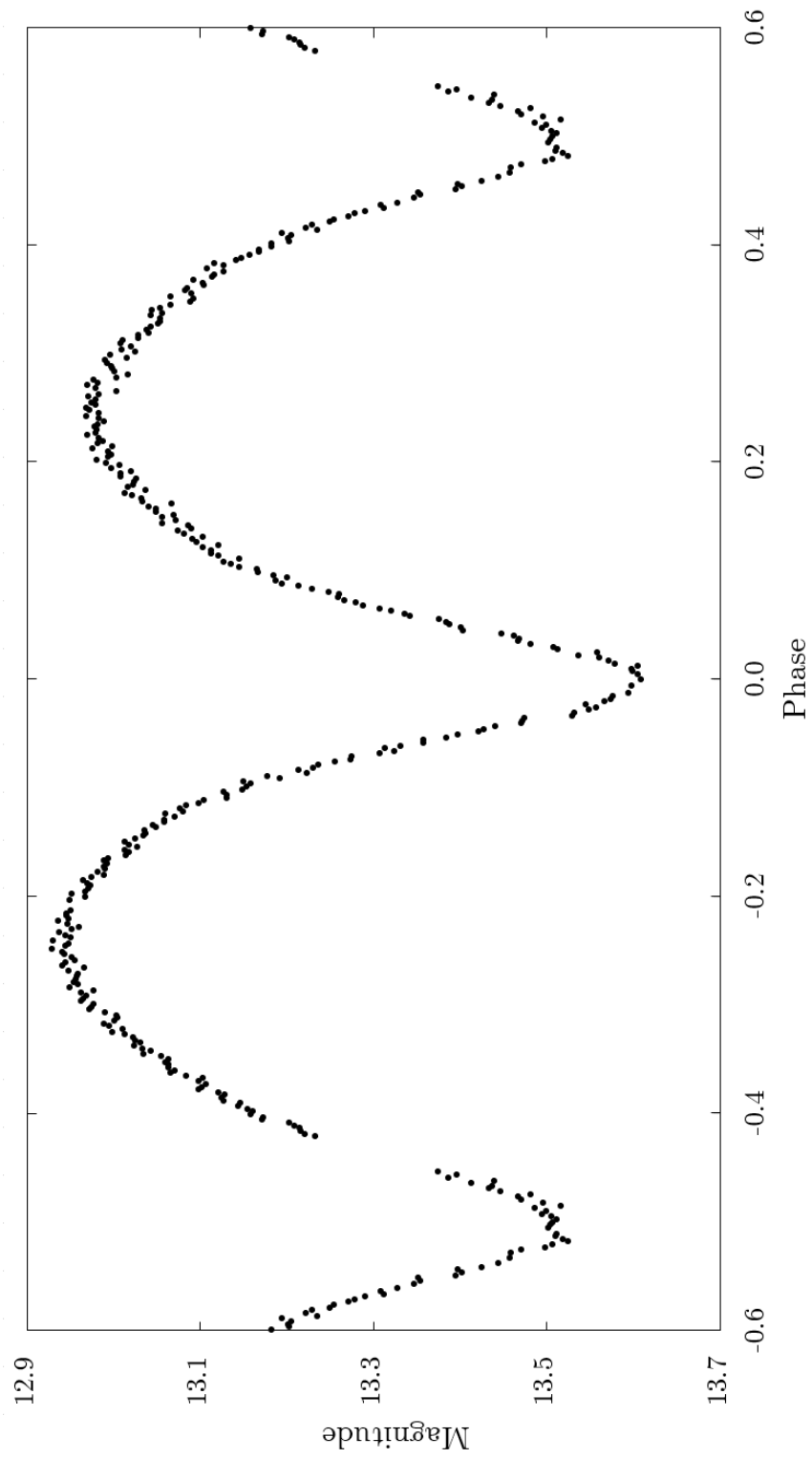
Figure A.12: Observational light curve of V574 Lyr from the night of 07/13/18 in the Sloan i' filter.

Figure A.13: Observational light curve of V574 Lyr from the night of 07/14/18 in the Sloan i' filter.
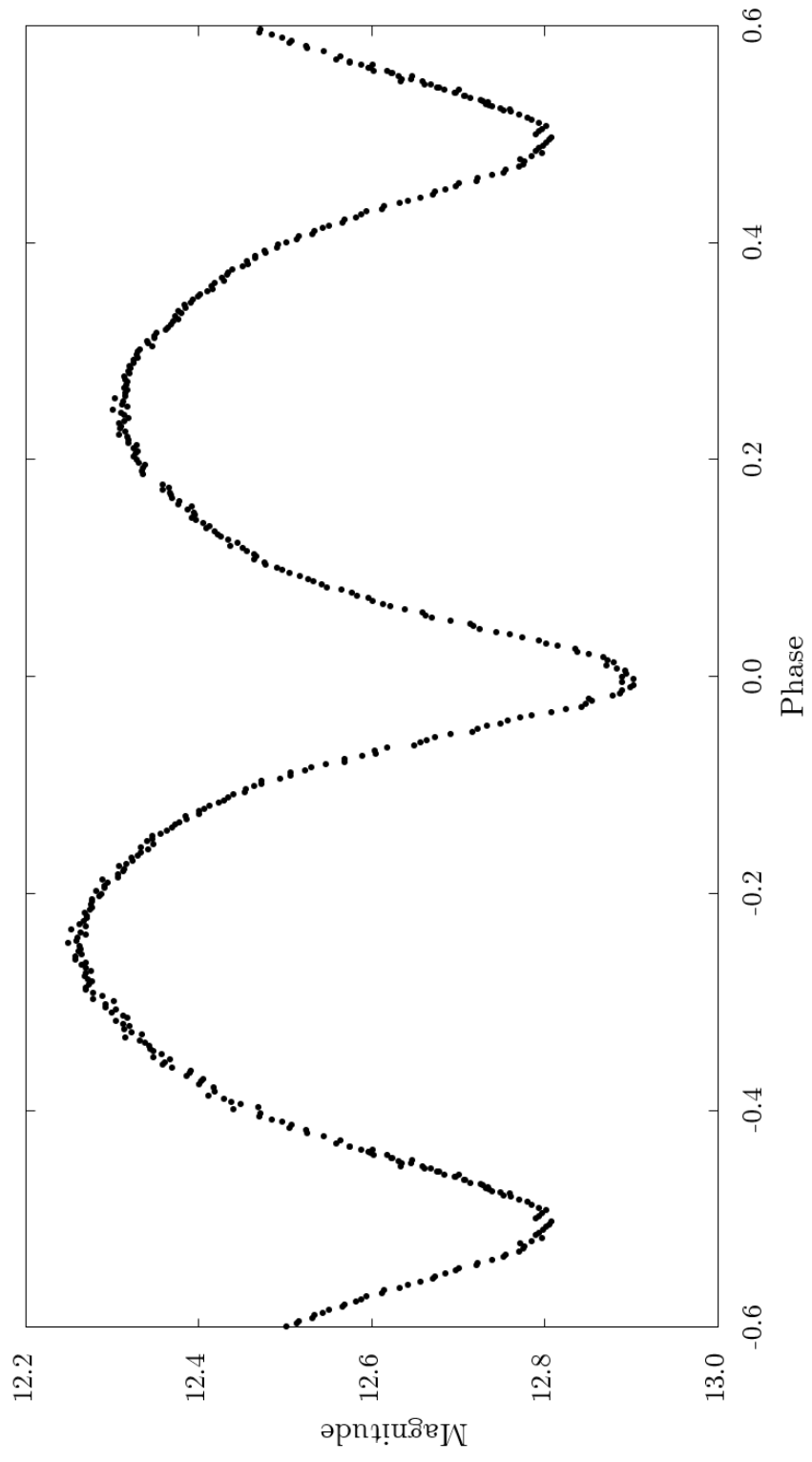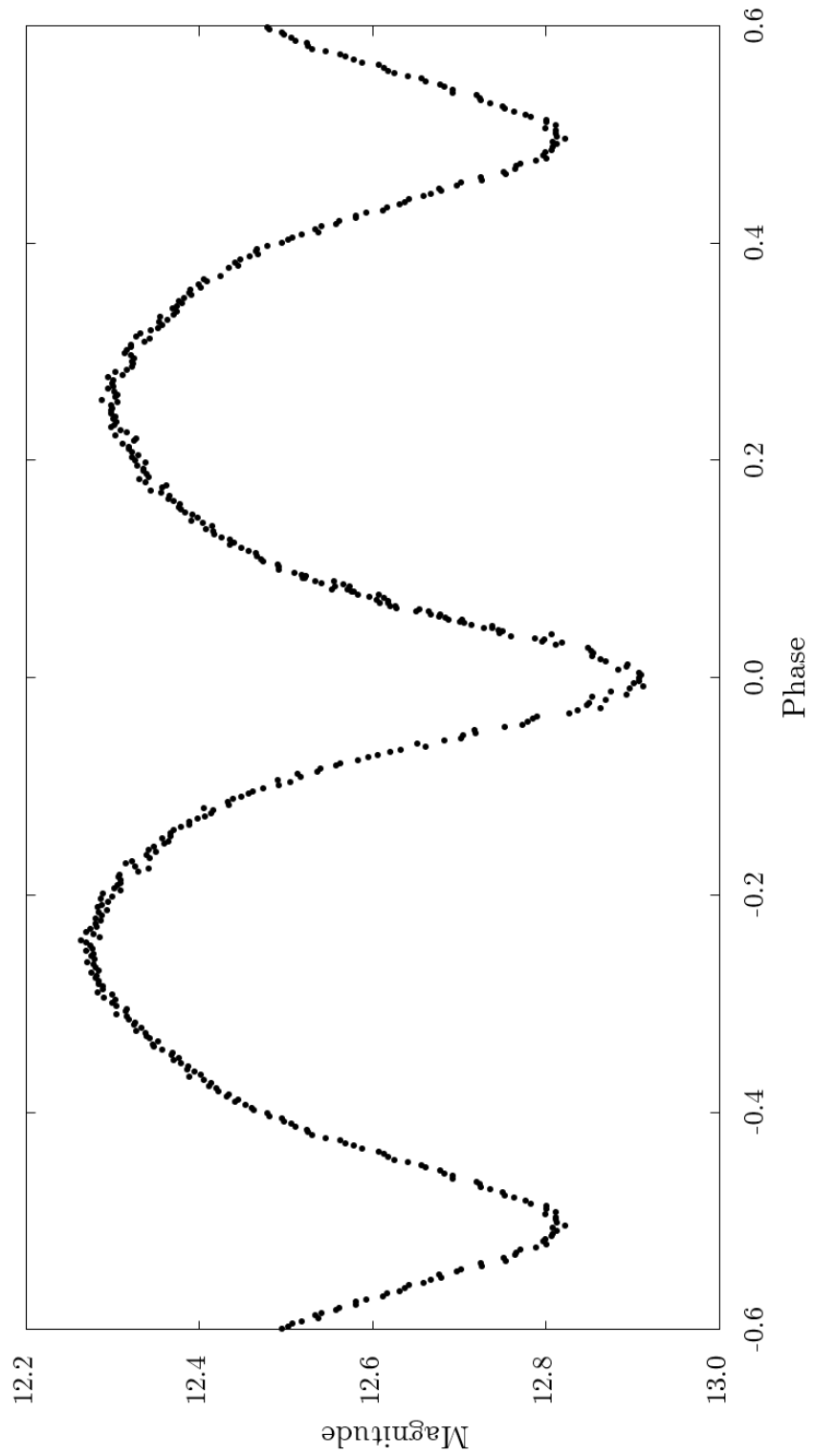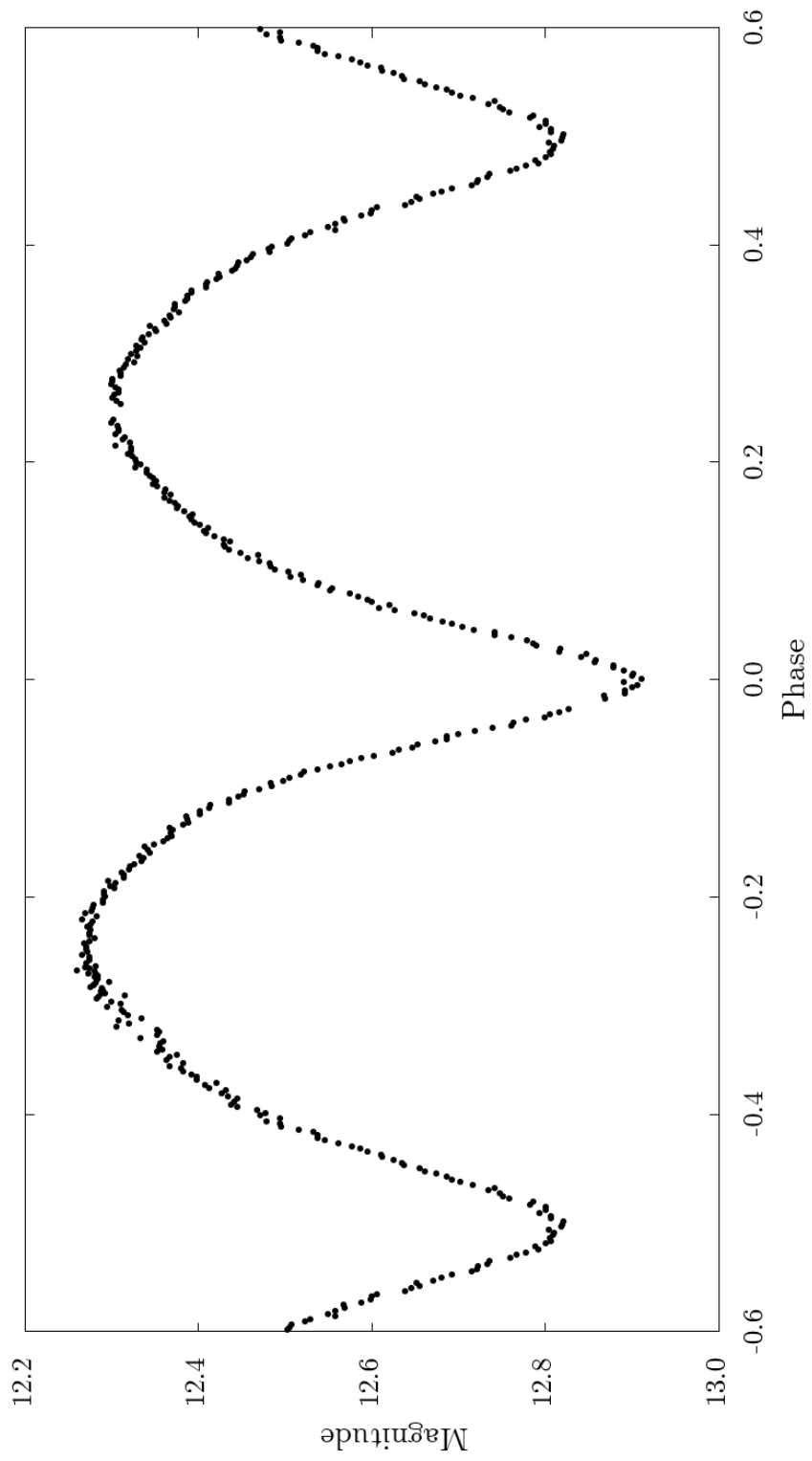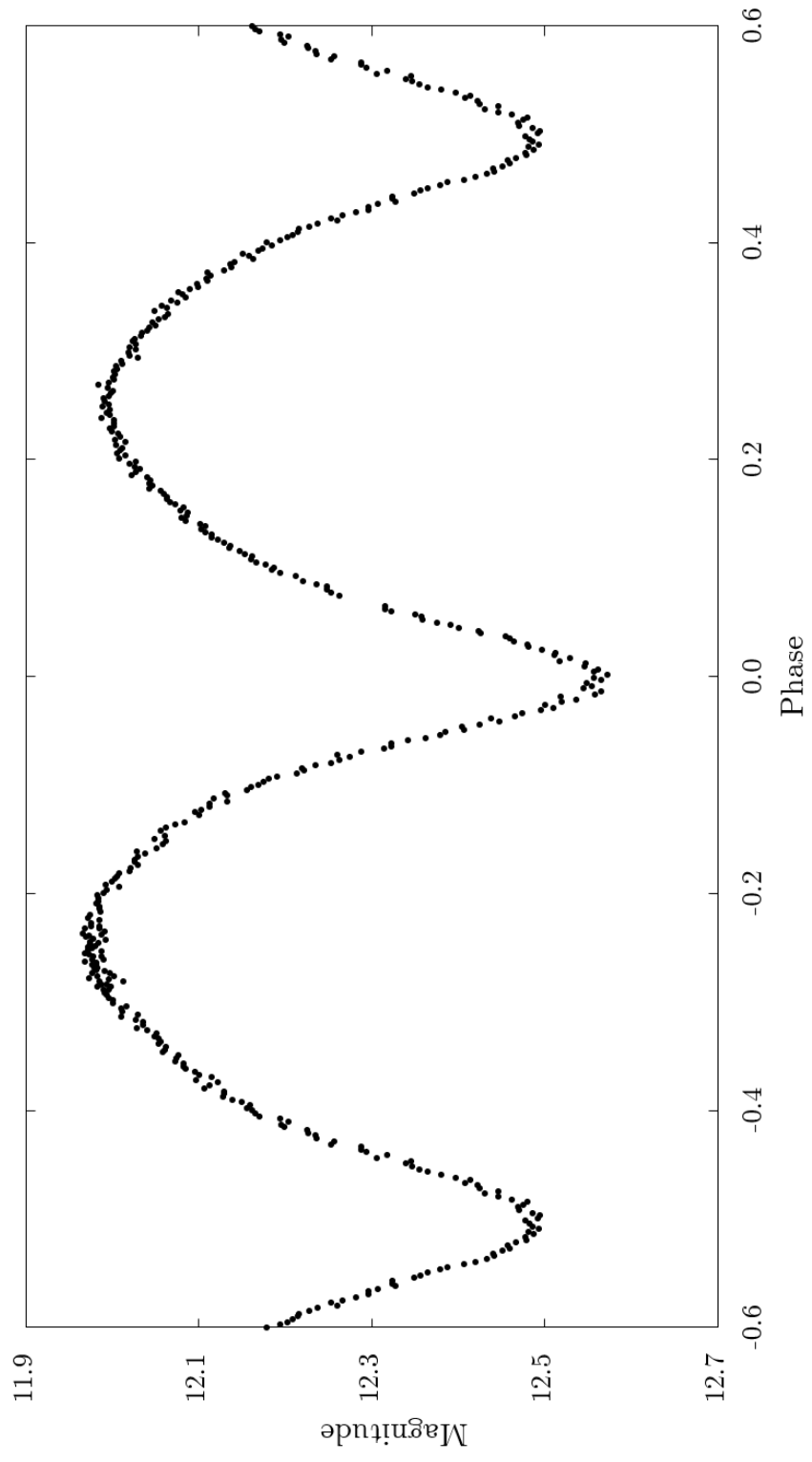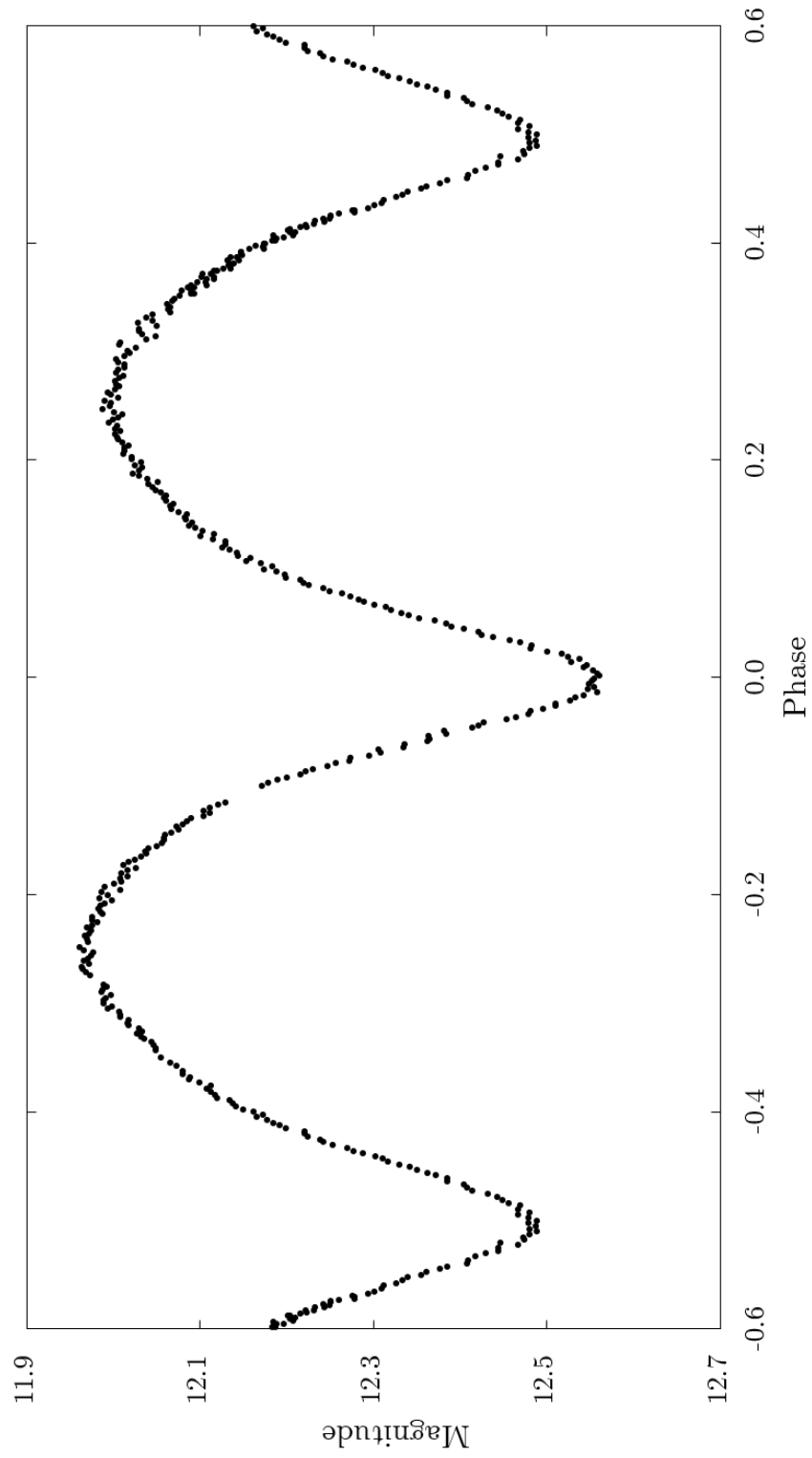
Times of Minima

APPENDIX B

Table B.1: Published and observed times of minima in HJD of V574 Lyr. Primary eclipses are denoted by Roman numeral I and secondary eclipses by Roman numeral II.

Type	Time of Minima (HJD)	Error (dys)	Source
II	2451260.88160		(Blättler and Diethelm 2000)
I	2451288.87970		(Blättler and Diethelm 2000)
II	2451757.42760	0.00070	(Blättler, *et al.* 2000)
I	2451757.56430	0.00240	(Blättler, *et al.* 2000)
I	2451768.48940	0.00060	(Blättler, *et al.* 2000)
I	2451773.40610	0.00070	(Blättler, *et al.* 2000)
II	2451781.46190	0.00020	(Blättler, *et al.* 2000)
I	2452116.45160	0.00060	(Blättler, *et al.* 2001)
I	2452443.38570	0.00070	(Blättler, *et al.* 2002)
I	2452783.42670	0.00130	(Diethelm 2003)
II	2453151.46440	0.00150	(Diethelm 2004)
I	2453229.44190	0.00020	(Hubscher, *et al.* 2005)
II	2453229.58030	0.00030	(Hubscher, *et al.* 2005)
II	2453256.34610	0.00040	(Hubscher, *et al.* 2005)
I	2453504.47975		(Brat, *et al.* 2007)
I	2453629.29750	0.00120	(Diethelm 2006a)
I	2453917.45010	0.00050	(Hubscher, *et al.* 2006)
II	2454018.36940	0.00090	(Diethelm 2006b)
I	2454295.45770	0.00060	(Hubscher 2007)
I	2454350.35500	0.00020	(Hubscher, *et al.* 2009)
I	2454354.72520	0.00010	(Nelson 2008)
II	2454384.36010	0.00080	(Diethelm 2008)
I	2454596.44250	0.00020	(Hubscher, *et al.* 2009)
I	2454596.57900	0.00340	(Hubscher, *et al.* 2009)
II	2455075.36882	0.00020	(Brat, *et al.* 2011)
II	2455104.31830	0.00120	(Diethelm 2010a)
I	2455104.45650	0.00090	(Diethelm 2010a)
II	2455156.21330	0.00020	(Brat, *et al.* 2011)
II	2455156.21380	0.00030	(Brat, *et al.* 2011)
II	2455312.44042	0.00030	(Brat, *et al.* 2011)
II	2455312.44092	0.00050	(Brat, *et al.* 2011)
II	2455336.74960	0.00030	(Diethelm 2010b)
I	2455336.88800	0.00300	(Diethelm 2010b)
II	2455430.43171	0.00020	(Brat, *et al.* 2011)
II	2455430.43261	0.00020	(Brat, *et al.* 2011)
II	2455461.29650	0.00050	(Brat, *et al.* 2011)

Continued on next page

Type	Time of Minima (HJD)	Error (dys)	Source
II	2455461.29710	0.00070	(Brat, *et al.* 2011)
I	2455643.60903	0.00020	(Honkova, *et al.* 2013)
I	2455643.60911	0.00010	(Honkova, *et al.* 2013)
I	2455643.60919	0.00020	(Honkova, *et al.* 2013)
I	2455673.38200	0.00170	(Hubscher, *et al.* 2012)
I	2455673.51670	0.00160	(Hubscher, *et al.* 2012)
II	2455691.54273	0.00010	(Honkova, *et al.* 2013)
II	2455691.54302	0.00020	(Honkova, *et al.* 2013)
II	2455691.54305	0.00010	(Honkova, *et al.* 2013)
I	2455712.43794	0.00020	(Honkova, *et al.* 2013)
I	2455712.43804	0.00030	(Honkova, *et al.* 2013)
I	2455712.43824	0.00030	(Honkova, *et al.* 2013)
II	2455791.50700	0.00030	(Banfi, *et al.* 2012)
I	2455794.37730	0.00050	(Honkova, *et al.* 2013)
I	2455795.46880	0.00030	(Banfi, *et al.* 2012)
II	2455798.33590	0.00030	(Banfi, *et al.* 2012)
I	2455798.47280	0.00040	(Banfi, *et al.* 2012)
II	2455799.42780	0.00100	(Banfi, *et al.* 2012)
I	2455800.38500	0.00070	(Banfi, *et al.* 2012)
II	2455800.51960	0.00100	(Banfi, *et al.* 2012)
II	2455801.33990	0.00030	(Banfi, *et al.* 2012)
I	2455801.47760	0.00040	(Banfi, *et al.* 2012)
II	2455802.43250	0.00050	(Banfi, *et al.* 2012)
II	2455984.60969	0.00020	(Honkova, *et al.* 2013)
II	2455984.60969	0.00020	(Honkova, *et al.* 2013)
II	2455984.60975	0.00010	(Honkova, *et al.* 2013)
I	2456044.56158	0.00030	(Honkova, *et al.* 2013)
I	2456044.56168	0.00010	(Honkova, *et al.* 2013)
I	2456044.56178	0.00020	(Honkova, *et al.* 2013)
II	2456062.45230	0.00170	(Hubscher and Lehmann 2013)
I	2456073.51270	0.00010	(Hubscher and Lehmann 2013)
II	2456078.83970	0.00040	(Diethelm 2012)
I	2456134.42190	0.00100	(Hubscher, *et al.* 2013)
II	2456134.55910	0.00160	(Hubscher, *et al.* 2013)
II	2456433.35506	0.00030	(Honkova, *et al.* 2013)
II	2456433.35531	0.00030	(Honkova, *et al.* 2013)
II	2456433.35581	0.00040	(Honkova, *et al.* 2013)
II	2456433.35926	0.00031	(Honkova, *et al.* 2014)
II	2456433.35951	0.00025	(Honkova, *et al.* 2014)
II	2456433.36001	0.00038	(Honkova, *et al.* 2014)
I	2456462.44824	0.00020	(Honkova, *et al.* 2015)
I	2456462.44835	0.00020	(Honkova, *et al.* 2015)
I	2456462.44872	0.00020	(Honkova, *et al.* 2015)
I	2456490.44400	0.00080	(Hubscher 2013)
II	2456524.31040	0.00020	(Lampens, *et al.* 2017)

Type	Time of Minima (HJD)	Error (dys)	Source
I	2456524.44800	0.00020	(Lampens, *et al.* 2017)
I	2456590.27364	0.00050	(Honkova, *et al.* 2015)
I	2456590.27459	0.00060	(Honkova, *et al.* 2015)
I	2456596.28107	0.00020	(Honkova, *et al.* 2015)
I	2456596.28158	0.00010	(Honkova, *et al.* 2015)
I	2456819.42744	0.00080	(Honkova, *et al.* 2015)
I	2456819.42761	0.00040	(Honkova, *et al.* 2015)
I	2456819.42862	0.00110	(Honkova, *et al.* 2015)
II	2456819.56235	0.00030	(Honkova, *et al.* 2015)
II	2456819.56321	0.00040	(Honkova, *et al.* 2015)
II	2456819.56328	0.00060	(Honkova, *et al.* 2015)
I	2456856.43600	0.00170	(Hubscher and Lehmann 2015)
I	2456871.45770	0.00050	(Hubscher and Lehmann 2015)
I	2457090.63946	0.00020	(Jurysek, *et al.* 2017)
I	2457090.63974	0.00020	(Jurysek, *et al.* 2017)
I	2457090.63976	0.00010	(Jurysek, *et al.* 2017)
II	2457105.52712	0.00020	(Jurysek, *et al.* 2017)
II	2457105.52740	0.00030	(Jurysek, *et al.* 2017)
II	2457105.52820	0.00030	(Jurysek, *et al.* 2017)
I	2457176.40151	0.00010	(Jurysek, *et al.* 2017)
I	2457176.40179	0.00010	(Jurysek, *et al.* 2017)
	2457256.42850	0.00070	(Hubscher 2016)
I	2457264.34974	0.00020	(Jurysek, *et al.* 2017)
I	2457264.34980	0.00020	(Jurysek, *et al.* 2017)
II	2457264.48530	0.00030	(Jurysek, *et al.* 2017)
II	2457264.48596	0.00020	(Jurysek, *et al.* 2017)
I	2457516.44454	0.00020	(Jurysek, *et al.* 2017)
I	2457516.44455	0.00020	(Jurysek, *et al.* 2017)
I	2457516.44477	0.00020	(Jurysek, *et al.* 2017)
I	2457576.53271	0.00010	(Jurysek, *et al.* 2017)
I	2457576.53291	0.00010	(Jurysek, *et al.* 2017)
I	2457576.53298	0.00010	(Jurysek, *et al.* 2017)
II	2457658.33463	0.00020	(Jurysek, *et al.* 2017)
II	2457658.33466	0.00030	(Jurysek, *et al.* 2017)
II	2457658.33494	0.00010	(Jurysek, *et al.* 2017)
II	2458282.70406	0.00005	(Rickards 2018)
I	2458284.75360	0.00004	(Rickards 2018)
I	2458285.84615	0.00005	(Rickards 2018)
II	2458285.70856	0.00004	(Rickards 2018)
I	2458286.66566	0.00005	(Rickards 2018)
II	2458286.80091	0.00004	(Rickards 2018)
I	2458313.70496	0.00005	(Rickards 2018)
II	2458313.84114	0.00005	(Rickards 2018)
I	2458314.79757	0.00004	(Rickards 2018)
II	2458314.66064	0.00004	(Rickards 2018)

Type	Time of Minima (HJD)	Error (dys)	Source
I	2458315.89035	0.00004	(Rickards 2018)
II	2458315.75290	0.00005	(Rickards 2018)
I	2458319.71411	0.00006	(Rickards 2018)
II	2458319.84992	0.00005	(Rickards 2018)
I	2458320.80653	0.00005	(Rickards 2018)
II	2458320.66926	0.00005	(Rickards 2018)
I	2458331.73153	0.00005	(Rickards 2018)
I	2458332.82435	0.00005	(Rickards 2018)
II	2458332.68679	0.00005	(Rickards 2018)
I	2458333.64364	0.00004	(Rickards 2018)
II	2458333.77951	0.00006	(Rickards 2018)

VITA

Abigail Rickards completed her homeschool high school degree in 2009 in Tyler, Texas, after which she enrolled at LeTourneau University in Longview, Texas. During her time at LeTourneau University she worked as a supplemental instructor of calculus-based physics and as an astronomy lab assistant. During the summers of 2011 and 2012, she also completed research over the design and operation of a radio telescope at LeTourneau University, and for the last half of the summer of 2012, she completed research in Loop Quantum Cosmology through a research experience for undergraduates at Louisiana State University in Baton Rouge, Louisiana. She received the degree of Bachelor of Science in Engineering Physics from LeTourneau University in May 2013. For the following four and a half years, she was employed as a high school physics teacher at the Brook Hill School in Bullard, Texas. In January 2018, she entered the Graduate School of Stephen F. Austin State University and received the degree of Master of Science in Natural Science with a concentration in Physics in May 2019.

Permanent Address: 2906 Crestwood Ln
          Kilgore, TX 75662

References were cited in the style of the Journal of the American Association of Variable Star Observers

This thesis was typed by Abigail L. J. Rickards.